

**UNCLASSIFIED**

**AD 419199**

**DEFENSE DOCUMENTATION CENTER**

FOR

**SCIENTIFIC AND TECHNICAL INFORMATION**

CAMERON STATION, ALEXANDRIA, VIRGINIA



**UNCLASSIFIED**

NOTICE: When government or other drawings, specifications or other data are used for any purpose other than in connection with a definitely related government procurement operation, the U. S. Government thereby incurs no responsibility, nor any obligation whatsoever; and the fact that the Government may have formulated, furnished, or in any way supplied the said drawings, specifications, or other data is not to be regarded by implication or otherwise as in any manner licensing the holder or any other person or corporation, or conveying any rights or permission to manufacture, use or sell any patented invention that may in any way be related thereto.

419199

ARL 63-150

**EFFECTS OF MECHANICAL AND THERMAL ELECTRODE PROPERTIES ON THE BEHAVIOR OF THE FLUID TRANSPIRATION ARC**

CATALOGED BY LDUU

AS AD No. \_\_\_\_\_

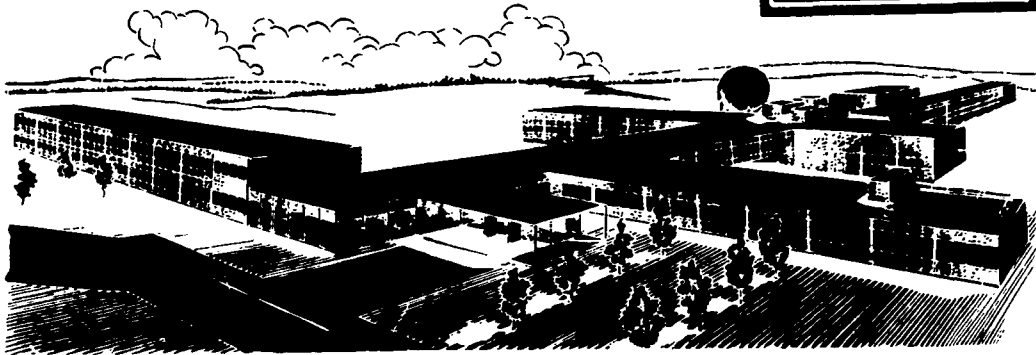
C. SHEER  
J. M. KENNEDY  
P. S. TSCHANG

COLUMBIA UNIVERSITY  
NEW YORK, NEW YORK

64-5  
419199

AUGUST 1963

AEROSPACE RESEARCH LABORATORIES  
OFFICE OF AEROSPACE RESEARCH  
UNITED STATES AIR FORCE



**NOTICES**

When Government drawings, specifications, or other data are used for any purpose other than in connection with a definitely related Government procurement operation, the United States Government thereby incurs no responsibility nor any obligation whatsoever; and the fact that the Government may have formulated, furnished, or in any way supplied the said drawings, specifications, or other data, is not to be regarded by implication or otherwise as in any manner licensing the holder or any other person or corporation, or conveying any rights or permission to manufacture, use, or sell any patented invention that may in any way be related thereto.

- - - - -

Qualified requesters may obtain copies of this report from the Defense Documentation Center, (DDC), Cameron Station, Alexandria, Virginia.

- - - - -

This report has been released to the Office of Technical Services, U. S. Department of Commerce, Washington 25, D. C. for sale to the general public.

- - - - -

Copies of ARL Technical Documentary Reports should not be returned to Aerospace Research Laboratories unless return is required by security considerations, contractual obligations or notices on a specified document.

ARL 63-150

**EFFECTS OF MECHANICAL AND THERMAL ELECTRODE  
PROPERTIES ON THE BEHAVIOR OF THE  
FLUID TRANSPIRATION ARC**

*C. SHEER  
J. M. KENNEDY  
P. S. TSCHANG*

*ELECTRONICS RESEARCH LABORATORIES  
SCHOOL OF ENGINEERING AND APPLIED SCIENCE  
COLUMBIA UNIVERSITY  
NEW YORK, NEW YORK*

AUGUST 1963

Contract AF 33(657)-8868  
Project 7063  
Task 7063-03

AEROSPACE RESEARCH LABORATORIES  
OFFICE OF AEROSPACE RESEARCH  
UNITED STATES AIR FORCE  
WRIGHT-PATTERSON AIR FORCE BASE, OHIO

## FOREWORD

This interim technical report was prepared by the Space Science Laboratory of the Electronics Research Laboratories, School of Engineering and Applied Science, Columbia University, New York, New York, on Contract AF 33 (657)-8868 for the Aerospace Research Laboratories, Office of Aerospace Research United States Air Force. The work reported herein covers the period from 1 May 1962 to 30 April 1963. The work was accomplished on Task 7063-03, "Energy Exchange Phenomena in Electric Arc Discharge" of Project 7063, "Mechanics of Flight".

The work described in this report has benefited from cooperation by the staff of Electronics Research Laboratories at large. Special acknowledgement is made of the contributions by C. Stojanoff and K. Weil in the design of the arc equipment and N. Pudliener in the electrode characterization program.

The project staff is also grateful for the helpful technical discussion with Mr. Eric E. Soehngen, Chief of the Thermo Mechanics Research Laboratory of ARL.

## ABSTRACT

The over-all objective of the present studies is to construct a satisfactory working model of the transpiration of a fluid medium through a porous anode into a DC electric arc. The emphasis is on the effects of electrode and working fluid properties on the energy transfer and arc characteristics under different conditions of transpiration flow rate and arc power.

The experimental work described includes physical characterization of several chosen porous anode materials in terms of porosity, pore structure, gas flow permeability, thermal conductivity, and local flow field studies. The construction of a flexible fluid transpiration arc test equipment is presented.

The first approach to the analytical studies of fluid transpiration cooling is described.

TABLE OF CONTENTS

SECTION	PAGE
I. INTRODUCTION	1
A. PURPOSE OF THIS REPORT	1
B. SCOPE OF THE PROJECT	
C. ACCOMPLISHMENTS DURING THE PERIOD COVERED BY THIS REPORT	2
D. DIRECTION OF FUTURE WORK	2
II. ANODE DEVELOPMENT	4
A. REQUIREMENTS ON PHYSICAL PROPERTIES OF POROUS MATERIALS SUITABLE FOR FLUID TRANSPIRATION	4
B. DESCRIPTION OF EXPERIMENTAL APPARATUS	5
C. DISCUSSION OF EVALUATED MATERIAL PROPERTIES	12
III. ARC ASSEMBLY DEVELOPMENT	39
A. GEOMETRY OF THE ARC ASSEMBLY: THE TRIPLE CATHODE GEOMETRY	39
B. DESIGN OF THE ARC ASSEMBLY	42
C. PROGRESS TO DATE IN THE FABRICATION OF THE ARC ASSEMBLY	42
D. INTERIM ARC ASSEMBLY	47
IV. ANALYTICAL UNDERTAKINGS	51
V. SUMMARY AND CONCLUSION	57
VI. REFERENCES	58

LIST OF FIGURES

FIGURE		PAGE
1	Gas Flow Permeability Measuring System (Schematic Diagram)	6
2	Sample Holder for Gas Flow Permeability Measurement	8
3	Local Flow Probe Assembly	10
4	Thermal Conductivity Measuring System	11
5	Gas Flow Rate Plots of Porous Tungsten Specimens for Argon	14
6	Gas Flow Rate Plots of Porous Tungsten Specimens for Helium	15
7	Gas Flow Rate Plots of Porous Tungsten Specimens for Nitrogen	16
8	Gas Flow Rate Plots of Porous Tungsten Specimens for Air	17
9	Specific Permeability, $K$ , in $10^{-8}\text{cm}^2$ for Spheroidized Tungsten Specimens	18
10	Photomicrograph: (140/170 mesh) Spheroidized Tungsten	19
11	Photomicrograph: (170/200 mesh) Spheroidized Tungsten	19
12	Photomicrograph: (200/325 mesh) Spheroidized Tungsten	20
13	Photomicrograph: (325/400 mesh) Spheroidized Tungsten	20
14	Photomicrograph: (200/325 mesh) Spheroidized Tungsten (showing plugged area)	21
15	Photomicrograph: (200/ mesh) Spheroidized Tungsten (showing plugged area)	21
16	Photomicrograph: (170/200 mesh) Spheroidized Tungsten (bushing sample)	22
17	Photomicrograph: (200/325 mesh) Spheroidized Tungsten (bushing sample)	22
18	Pore-Size Distribution: Spheroidized Tungsten (140/170 mesh)	24

LIST OF FIGURES (CONT'D.)

FIGURE		PAGE
19	Pore-Size Distribution: Spheroidized Tungsten (170/200 mesh)	25
20	Local (Cold) Flow Probe Variation of Porous Specimens	26
21	Gas Flow Rate Plots	27
22	Gas Flow Rate Plots	28
23	Photomicrograph: NC 50 Graphite	29
24	Photomicrograph: NC 50 Graphite	29
25	Photomicrograph: NC 50 Graphite	29
26	Photomicrograph: NC 60 Graphite	30
27	Photomicrograph: NC 60 Graphite	30
28	Photomicrograph: NC 60 Graphite	31
29	Photomicrograph: NC 60 Graphite	31
30	Photomicrograph: NC 60 Graphite	32
31	Photomicrograph: NC 60 Graphite	32
32	Pore-Size Distribution: NC 50 Graphite	33
33	Pore-Size Distribution: NC 60 Graphite	34
34	Photomicrograph: PC-57	36
35	Photomicrograph: PC-59	36
36	Photomicrograph: Feltmetal 90 Per Cent Porosity Type A Fiber, 302 Stainless Steel	37
37	Photomicrograph: Feltmetal 90 Per Cent Porosity Type A Fiber, 302 Stainless Steel	37
38	Pore-Size Distribution: Feltmetal 90 Per Cent Porosity Type A Fiber, 302 Stainless Steel	38
39	Geometry of Cathode Jets and Transpired Gas Flow with Cathodes in Swept Back Position	40

LIST OF FIGURES (CONT'D.)

FIGURE		PAGE
40	Typical Operation of Triple-Cathode Arc Assembly	41
41	Cathode Motion	43
42	Triple-Cathode Arc Assembly (Showing one of the three cathode mechanisms)	44
43	Photograph of Parts for Triple-Cathode Arc Assembly	45
44	Photograph of Parts for Triple-Cathode Arc Assembly (Showing arrangement for the Sub-Assemblies)	46
45	Interim Arc Assembly	48
46	Simplified Arc Assembly for Test of Sintered Spheroidized Tungsten Anode	49
47	Local Flow Probe Measurement: Interim Arc Assembly	50
48	One-Dimensional Fluid Transpiration Cooling, Case I	53
49	One-Dimensional Fluid Transpiration Cooling, Case II	54
50	One-Dimensional Fluid Transpiration Cooling, Case III	55

## I. INTRODUCTION\*

### A. PURPOSE OF THIS REPORT

The purpose of this report is to describe the work accomplished under Contract AF-33(657)8868, during the period May 1, 1962 through April 30, 1963, the initial twelve months of research under the contract. In this introductory section the scope of the project is set forth, the major accomplishments of the report period are briefly reviewed and the direction of the future work is indicated. In subsequent sections the work done during the period of the report is discussed in detail.

### B. SCOPE OF THE PROJECT

The aim of this project is to conduct an analytical and experimental investigation of the thermal, electrical and mechanical phenomena which characterize the transpiration of a fluid medium through a porous anode into a DC electric arc. The objective is to develop a satisfactory working model to explain the observed behavior of the arc under varying conditions of fluid flow rate, arc current, ambient pressure and the chemical, thermal and mechanical properties of both fluid medium and porous electrode.

The investigation places particular emphasis on a study of the effects of electrode and working fluid properties on energy transfer and arc characteristics. Performance criteria for this study consist of energy transfer efficiency, arc terminal characteristics, total effluent plasma enthalpy and rate of electrode ablation.

The investigation includes the following electrode parameters:

- porosity and pore geometry;
- pore size and homogeneity;
- gas flow permeability;
- thermal conductivity;
- electrode composition.

Time permitting, the objectives of the project include initiating research in two additional areas. First, a study of the power-handling capability of high-performance electrodes is to be undertaken. Second, the effects of the micro-flow field within the anode sheath on arc terminal characteristic, arc stability, and energy partition between electrode and effluent plasma are to be studied. Analytically this study is to develop a theoretical description of the effluent flow field close to the electrode surface, taking into account nonuniformity of fluid flow due to non-uniform temperature distribution across the active electrode surface. Experimental verification of the analysis by empirical determination of an energy balance for the porous anode is to be attempted.

---

\* Manuscript released June 1963 by the authors for publication as an ARL Technical Documentary Report.

### C. ACCOMPLISHMENTS DURING THE PERIOD COVERED BY THIS REPORT

The principal effort under this project falls naturally into two parts, viz., investigation of electrode properties; and investigation of arc properties.

To investigate electrode properties five experiments were designed and the experimental apparatus constructed or purchased.

- (1) An Aminco-Winslow mercury porosimeter was purchased and put in operation. This device measures the porous volume of a sample accessible through pores of a given size.
- (2) An apparatus was constructed to measure the gas flow permeability of samples.
- (3) Apparatus was constructed to measure the thermal conductivity of samples.
- (4) Photomicrographic examination of samples was performed to investigate the homogeneity and connectivity of pore sizes in anode materials.
- (5) Local gas flow probes were used to investigate the homogeneity of gas flow near the surface of porous samples.

This experimental equipment is described in detail in Sec. II-B and the results of tests on samples of a variety of porous materials are discussed in Sec. II-C. Several varieties of porous graphite have been studied as well as several varieties of sintered spheroidized tungsten. Some preliminary tests have also been made on felted stainless steel.

The investigation of arc properties requires an arc apparatus with certain requirements of geometrical flexibility and adaptability to diagnostic instrumentation. During the period covered by this report such an assembly was designed and constructed. This apparatus is at present being assembled and should be in operation in the very near future. Its functioning and design are discussed in Sec. III. Also included in Sec. III is a description of some simplified arc assemblies which were used for interim tests on promising anode materials.

Section IV contains a description of the preliminary analytical work performed in the period covered by this report. This examination of the gas and thermal flow fields in and near the electrode is directed toward the study of the effects of the micro-flow field in the anode sheath on arc characteristics.

### D. DIRECTION OF FUTURE WORK

In addition to continuing the study of sintered spheroidized tungsten, tests will be conducted on other possible anode materials.

Among these may be mentioned felted metal strands which have shown some promise in preliminary tests. Tests are currently being performed on felted stainless steel with porosities in the range of 40 per cent to 90 per cent. Similarly manufactured materials of more refractory metals are available and will be investigated if the mechanical properties of the felted stainless steel prove satisfactory. In addition some investigation of woven tungsten fibers may be performed although this type of material is somewhat more expensive than the materials currently under investigation and study of the former will be given lower priority.

The arc assembly should presently be in operation and the availability of this device will permit correlation of the results of tests on porous materials with the performance of these materials in actual arc burning tests. After shakedown and determination of the arc characteristics at atmospheric pressure, present plans call for construction or purchase of a chamber which will permit operation of the arc assembly at pressures below and above atmospheric. Protective, monitoring, control and recording equipment for the arc assembly is currently being designed or constructed, as is diagnostic equipment. In particular a high-speed probe is under construction; this device will be used for electrical and thermal probing of the arc. Design of a calorimetric experiment for determining energy balance in the arc will be begun presently.

## II. ANODE DEVELOPMENT

### A. REQUIREMENTS ON PHYSICAL PROPERTIES OF POROUS MATERIALS SUITABLE FOR FLUID TRANSPIRATION

To fulfill the mission of bringing about energy transfer from the arc to the transpiring fluid, the porous medium can be considered of high performance only if it can preserve itself against thermal destruction while causing maximum energy transfer to the fluid medium. To serve as an anode, it must be electrically conducting, although, in contrast to the case of solid electrodes, the electrical resistivity needs not be minimized, since a major portion of the ohmic power is introduced to the fluid. The volume heat transfer coefficient between the material and the fluid must be high and at the same time the flow permeability should also be high to permit high mass flow transfer. The material should have good thermal strength in the porous state which means high intrinsic melting point and thermal shock resistance, as well as structural rigidity. To prevent structural failure due to excessive temperature gradients, it should have high thermal diffusivity which generally depends on high thermal conductivity. Finally, the above mentioned properties should be distributed homogeneously within the material to prevent local failure from starting and spreading. This is especially important in view of the fact that the arc column tends to seek out and terminate on the hotter part of the electrode. There is yet another requirement that the pores in the material should be small in comparison with the postulated anode sheath thickness (of the order of 40 microns at atmospheric pressure) so that a continuous sheath may form, instead of one punctured by multiple effluent fluid streams.

The above stated requirements are not all independent of one another. Some properties are difficult to measure independently, e.g., volume heat transfer coefficient, and can be best evaluated during the running of the arc. Nevertheless, more or less independent experiments were designed to obtain the following parameters:

- (1) Porosity
- (2) Thermal Conductivity
- (3) Flow Permeability
- (4) Structural Homogeneity
- (5) Flow Homogeneity.

The details of the test apparatus are given below. The results of some of the specimens evaluated will be described in Sec. II-C of this report. It should be mentioned at this point two things to bear in mind before proceeding. First, the results to follow are but partial in a continuing program of anode material selection and evaluation. Secondly, actual performance of the anodes under arc test will provide the ultimate validation.

## B. DESCRIPTIONS OF EXPERIMENTAL APPARATUS

### 1. Description of Gas Flow Permeability Measuring System

In order to determine the gas flow permeability of porous specimens one must determine the gas flow rate through a sample and the pressure difference between upstream and downstream. Figure 1 is a schematic representation of the apparatus for determining gas flow permeability. Compressed gas is introduced through a regulator to the test sample holder. The exit gas is then passed through a Fischer and Porter Tri-Flat flowmeter before exhausting into the atmosphere. Two static pressure ports, upstream and downstream of the specimen, are connected to a Heise gauge and a U-tube mercury manometer in such a way that the following pressure readings may be obtained:

- (1) Upstream gauge pressure by Heise gauge
- (2) Upstream gauge pressure by U-tube
- (3) Differential pressure across sample by U-tube
- (4) Differential pressure from downstream to atmosphere (downstream gauge pressure) by U-tube.

The Heise gauge has a range of 0-10,000 mm of Hg and the U-tube has a range of 0-1000 mm of Hg.

The flowmeter yields indirect measurement of gas flow rate and may be as accurate as the calibration available since the Tri-Flat tubes of the flowmeter have high precision, allowing little wobbling and practically no resistance to the spherical float. Aside from parallax errors in reading the scales these flowmeters have yielded highly repeatable readings. One way of calibrating the flowmeter is to connect it in series with another one of known calibration. This requires availability of calibrating flowmeter covering the same range as that to be calibrated. Another method is through volumetric determination, either by graduated cylinders or volume displacement meter, over a known interval of time. A complete calibration of all flowmeter tubes and floats by the second method would be exceedingly time-consuming and therefore it was decided to make such measurements on a few points to gain some assurance as to their absolute accuracy. The final calibration curves were arrived at in the following way:

- (1) Initial calibrations were computed in accordance with Fischer and Porter Handbook 10A9010, taking into account density and viscosity of gas, tube size, float size and density
- (2) The computed values were smoothed
- (3) Experimental runs were made with the various tubes and floats
- (4) Where the curves obtained failed to meet, one was arbitrarily chosen as the norm and the other calibrations were adjusted to result in a continuous calibration curve over all ranges.

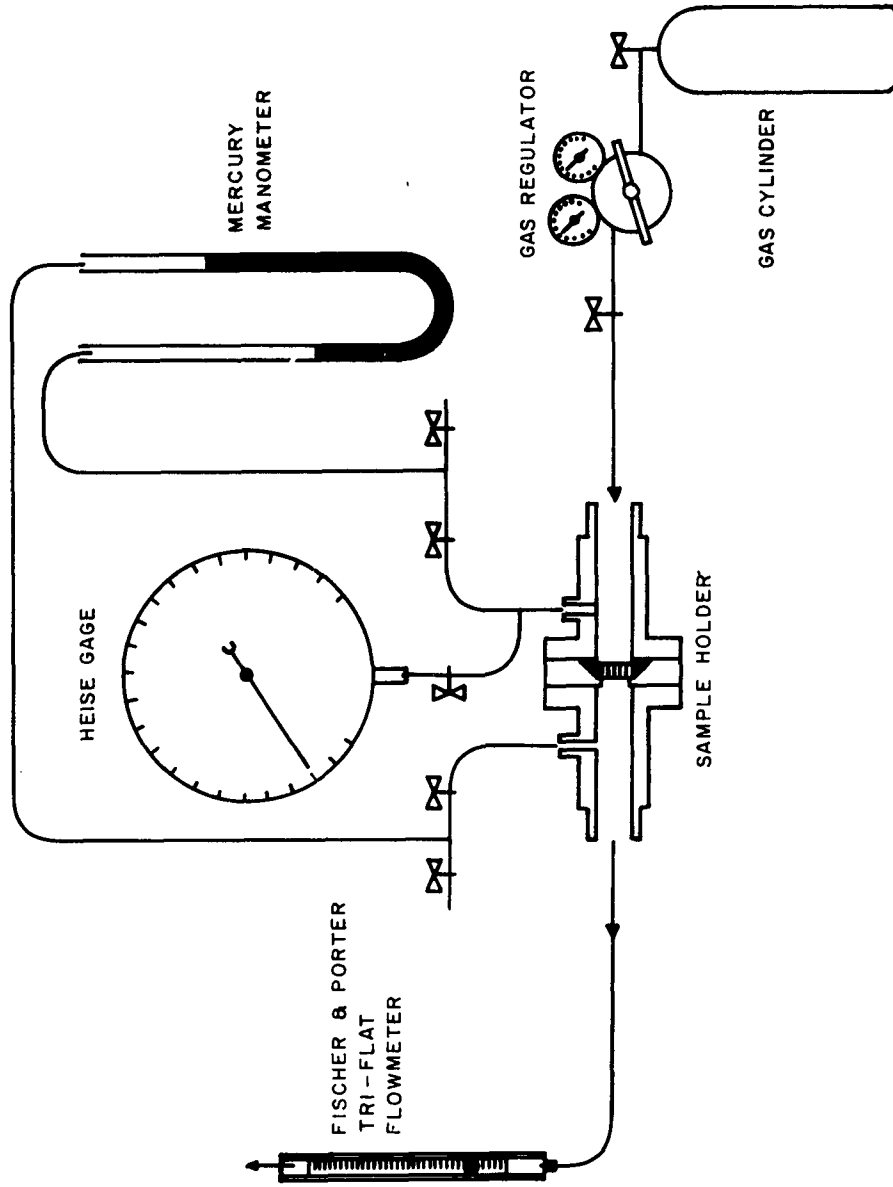


Fig. 1 Gas Flow Permeability Measuring System  
(Schematic Diagram)

The construction of the porous sample holder is shown in Fig. 2. The sample measuring 1/2 in. diameter by 1/8 in. thick is held against the gas stream by a slight constriction of the center ring. Leakage along the curved surface of the sample is prevented by a tapered Silicone rubber ring. Detection of leakage was not possible with the porous sample in place but when a solid piece was inserted no trace of escaping gas was detected. The static pressure ports are placed sufficiently close to the sample for essentially true pressure drop determination.

## 2. Photomicrography

A series of photomicrographs has been taken of the surface of the sintered tungsten specimens to study the porous structures. A positive means of estimating the size and shape of the pore opening as well as surface inhomogeneities was thus established.

To facilitate study of pore structures below the surface, plastic impregnation techniques have been developed. This involves preparation of the porous specimens by cutting and polishing for subsequent photomicrography. Specifically, porous graphite specimens are prepared by immersing them in a polyester (American Cyanamid Laminac 4110) which had been made extremely inviscid by the addition of methyl-ethyl-ketone peroxide (50 per cent by volume). After several hours of curing at room temperature the specimens are cut to expose the interior of the specimen, polished with emery cloth and finished with silver polish. The exposed graphite-plastic surface is then etched lightly with acetone to remove some of the plastic. Finally a thin coat of carbon black is applied to the surface with a butane flame to improve the contrast between the plastic and the graphite. Photographs have been taken with a Polaroid-Land camera through a Bausch and Lomb microscope at incident light grazing angles of approximately 30 deg to 60 deg.

## 3. Pore Size Distribution

Work in this area has been centered around the use of the AMINCO-Winslow Porosimeter for mercury penetration of the pore volume in the porous materials. Pressures ranging from a few mm of Hg to 5000 psi were applied to the porous material immersed in mercury and the resulting volume penetration read from a graduated stem. Since higher pressures are required to penetrate smaller pores, the differential volume penetrated under a given pressure can be plotted against the pore size which yields to penetration at that pressure. This gives the pore size distribution over all connected pores. Using this procedure samples of different grades of porous graphites and sintered spheroidized tungsten, made especially for use as anodes, have been tested.

## 4. Description of Local Flow Probe System

The homogeneity of the porous material for fluid transpiration application is reflected to a large extent in the local flow condition

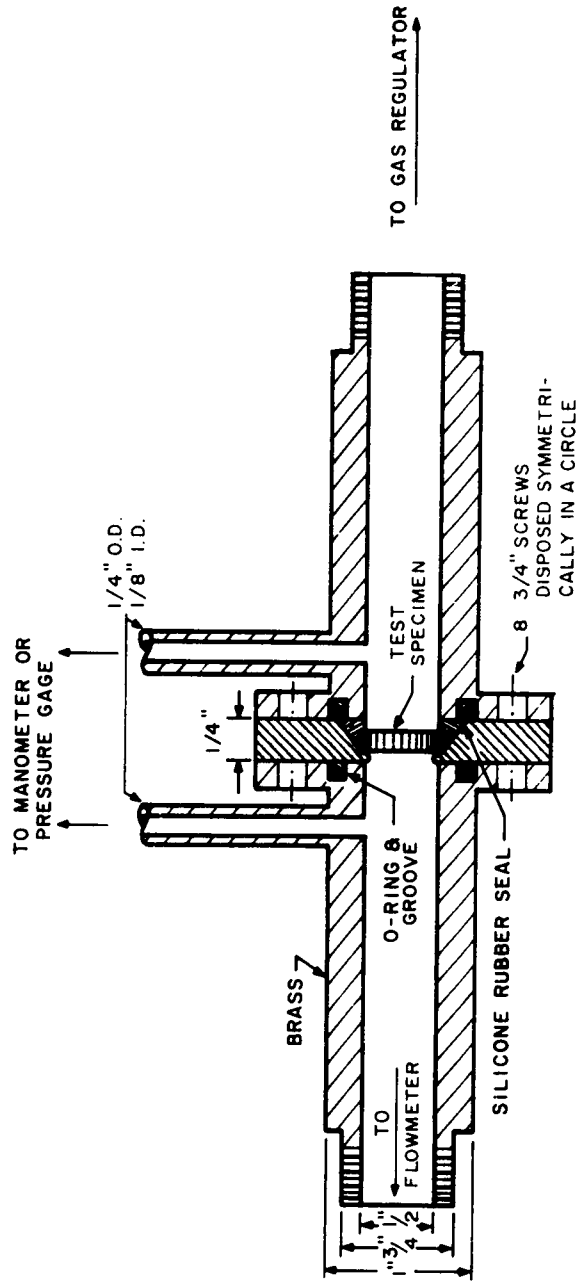


Fig. 2 Sample Holder for Gas Flow Permeability Measurement

of exhausting gas. Earlier a pressure probe and traverse arrangement was improvised for qualitative study of the local flow field and the results were significant enough to justify building a more permanent setup of higher precision and flexibility which can give quantitative data for the porous media.

The new apparatus, at present, nearly completed, is shown in perspective in Fig. 3. The probe is mounted on a two-degree-of-freedom rack-and-pinion drive which is secured to a cross arm which slides vertically along a dove-tailed groove. The probe is interchangeable and may be either straight or oriented at an angle as shown. In the latter case the probe may be rotated to point at orthogonal directions for data which when combined with the straight probe data can, in principle, give a complete determination of flow vector at each location. The porous anode holder is mounted on a standard rotary table which also has two degrees of linear freedom with the result that the total assembly allows probing to be done circularly as well as in the three linear directions.

The receptacle for the anode is designed such that complete anode holder from the arc system may be readily mounted here for testing before and after the arc run.

It is worth noticing that the physical dimension of the probe (approximately 0.02 in) permits the detection of macroscopic flow variations only.

##### 5. Description of Thermal Conductivity Measuring System

The measurement of the thermal conductivity of any material is based on the determination of the heat flux through a specimen of constant cross section and the temperature difference across it. If necessary, the system can also be adapted to use the comparison method of determining thermal conductivity whereby a standard specimen of known thermal conductivity is placed in a series with the unknown specimen and then the temperature drops across both pieces taken at the same instant.

The essential features of the system are indicated in Fig. 4. The heat source consists of Nichrome wires wound on a grooved toroid of boron nitride and then encapsulated in high temperature cement within a copper housing. Insulating and conducting materials are used in such a way as to facilitate quick removal of up to 1 kw of heat power from the heating elements towards the test sample. The specimen, suitably prepared, is placed between the heater and the heat sink, the latter being simply water cooled. Insulation is used around the apparatus to minimize radial heat loss. It was found necessary to apply several hundred pounds per square inch of pressure on the specimen in order that a large heat flux be made to flow through it. The mechanism for exerting such pressures is not shown in the figure. Miniature Chromel-Alumel thermocouples are placed inside the heater and cooler to sense the temperatures on the heat conduction surfaces. Because this arrangement of thermocouples is

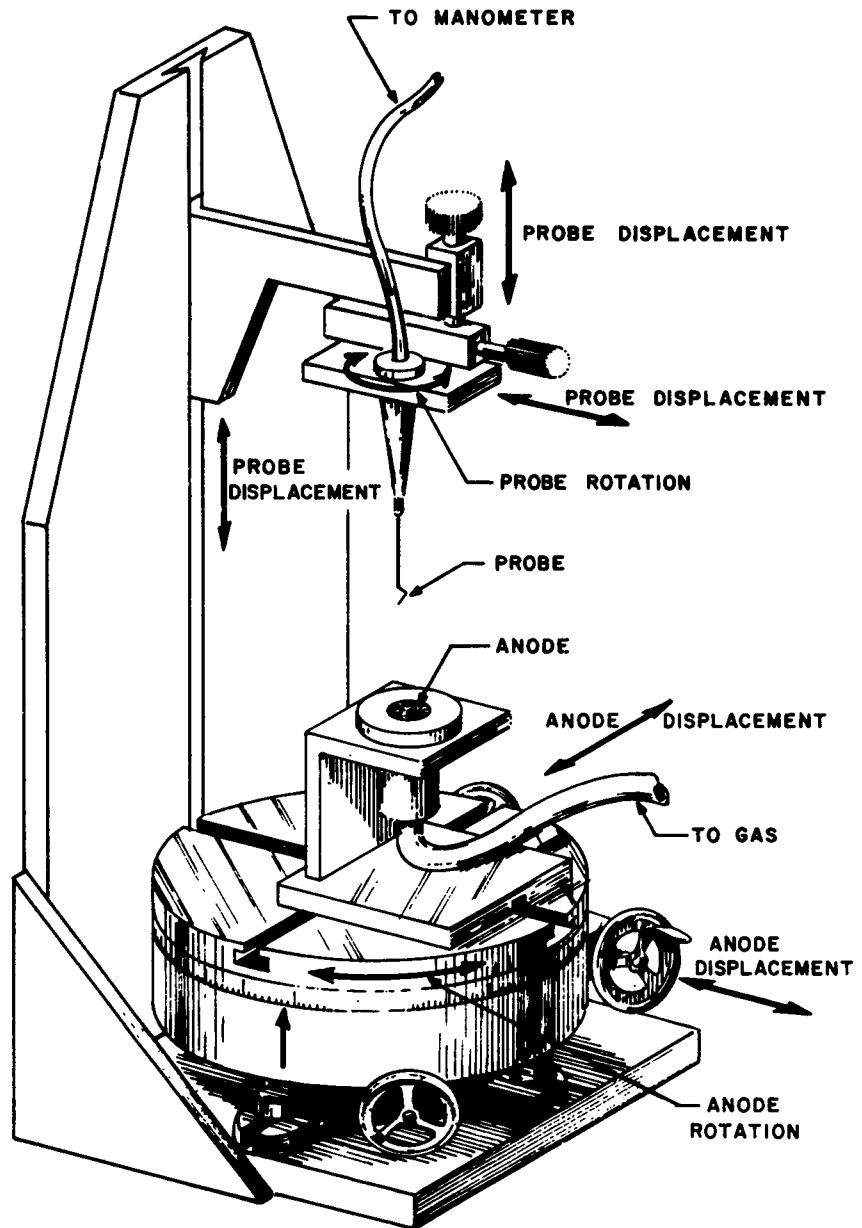
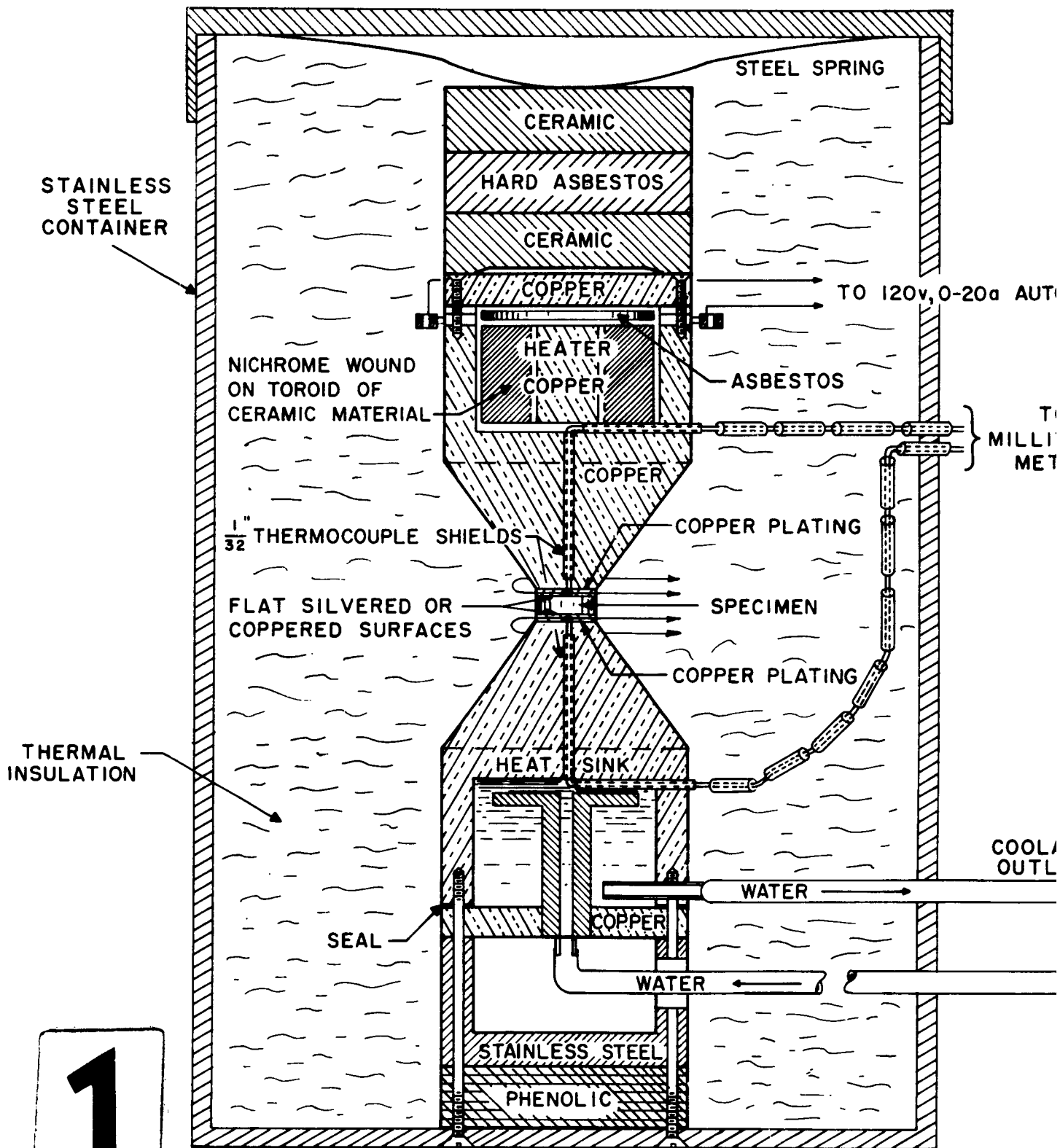


Fig. 3 Local Flow Probe Assembly



1

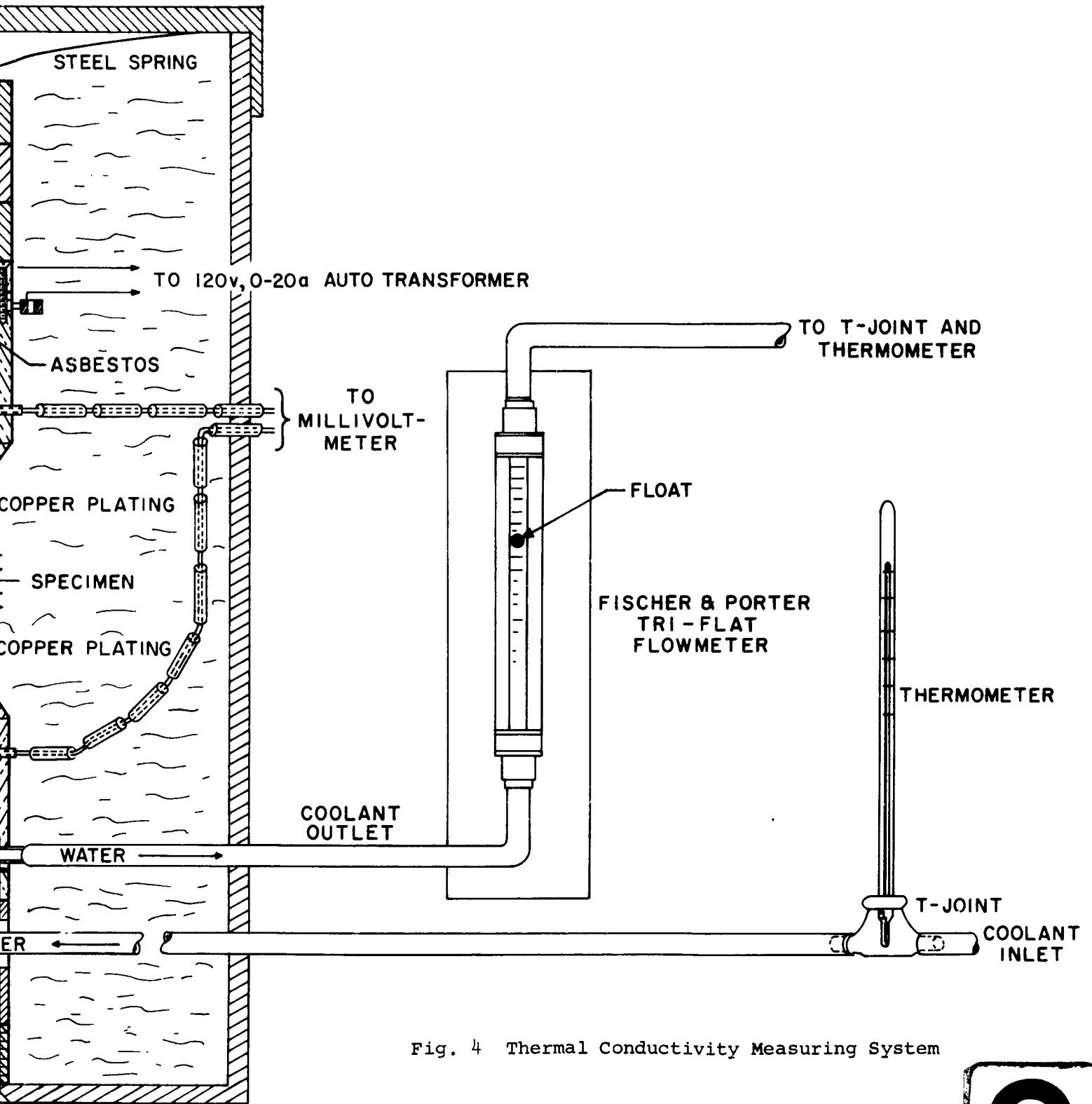


Fig. 4 Thermal Conductivity Measuring System

difficult to service and because of large inter-face temperature drops later measurements have been made with thermocouples imbedded in slots in a thin film of copper electro-plated on the surface of the specimens. The added pair of thermocouples are also shown in Fig. 4. All thermocouple outputs are taken to reference junctions (usually held at 0°C) and then to a Leeds and Northrup potentiometer. The inlet and exit water temperatures are measured by ordinary laboratory mercury thermometers. Water flow rate is monitored by a Fischer and Porter Tri-Flat flowmeter but final measurements are always taken with a graduated cylinder over a set time interval.

To give some indication of the efficiency with which the heater is able to introduce heat to the specimen, the electrical input is monitored with a voltmeter and an ammeter.

### C. DISCUSSION OF EVALUATED MATERIAL PROPERTIES

The general procedure in selecting materials for possible application as anodes is illustrated roughly in the following sequence:

- (1) First, flow permeability is tested. This is done first not only because reasonable flow rate with moderate pressure drop is desirable but also because a porous material which is not very permeable to flow due to predominance of deadend pores is likely to be undesirable also in terms of thermal conductivity, volume heat transfer coefficient, and mechanical strength.
- (2) Next, photomicrographs are taken of the surface structure to examine the pore outlets for size and homogeneity.
- (3) Then, mercury porosimeter tests are performed to determine the distribution of pore sizes and to determine the total and connected porosities.
- (4) Finally, thermal conductivity and
- (5) Flow probe tests are performed.

The last test is of crucial importance and should be performed with the same anode holder as that used in the subsequent arc burning test since it has been observed (cf. Sec. III-D) that thermal damage subsequently occurred locally in those regions where little or no gas emerged from the surface. The materials investigated up to this point include sintered spheroidized tungsten (4 mesh sizes), National Carbon NC-50, NC-60, Stackpole PC-57, PC-59 graphites and Huyck stainless steel Feltmetal.

#### 1. Sintered Spheroidized Tungsten

This seems to be the most promising material to date studied. Four sizes of spheroidized tungsten were used for hot pressing both circular discs and cylindrical bushings:

<u>U. S. Mesh</u>	<u>Microns</u>
140/170	105-88
170/200	88-74
200/325	74-44
325/400	44-37

The gas flow permeabilities of the disc specimens were given extensive measurements. In all cases the permeabilities were highly satisfactory as is evidenced in Figs. 5 through 8 for argon, helium, nitrogen and air, respectively. Using argon, for instance, even with the finest mesh size (325/400) 100 liters/min. (approximately 200 gm/min.) flow can be obtained at a pressure drop of about 2000 mm of Hg for specimens 3.2 mm thick and 1.26 cm<sup>2</sup> in area. These curves show that Darcy's law is not strictly valid throughout all ranges. Nevertheless, one can compute the specific permeability, defined as

$$k = \frac{\mu Q}{A \Delta p} \text{ cm}^2$$

where

- $\mu$  = viscosity in poise
- $Q$  = flow rate in cm<sup>3</sup>/sec
- $h$  = length in cm
- $A$  = area in cm<sup>2</sup>
- $\Delta p$  = pressure drop in dynes/cm<sup>2</sup>

Since  $k$  would vary slightly, calculations have been arbitrarily made at a pressure drop of 500 mm of Hg and tabulated in Fig. 9 for future reference. From the table it is apparent that  $k$  is a property of the porous material and is quite insensitive to the particular gas used.

Figures 10 to 17 are the photomicrographs of the tungsten specimens. Although the packing of the spheres are not wholly regular, the apparent homogeneity on an overall basis seems encouraging. This will become more evident as one examines the other porous materials. The apparent pore openings of the finer mesh size specimens are quite small, being in the vicinity of 10 microns or so. Figures 14 and 15 are photographs of a plugged specimen. As evidence that plugging may be inside also, its flow permeability is below normal, see Fig. 5 for 200/325 A.

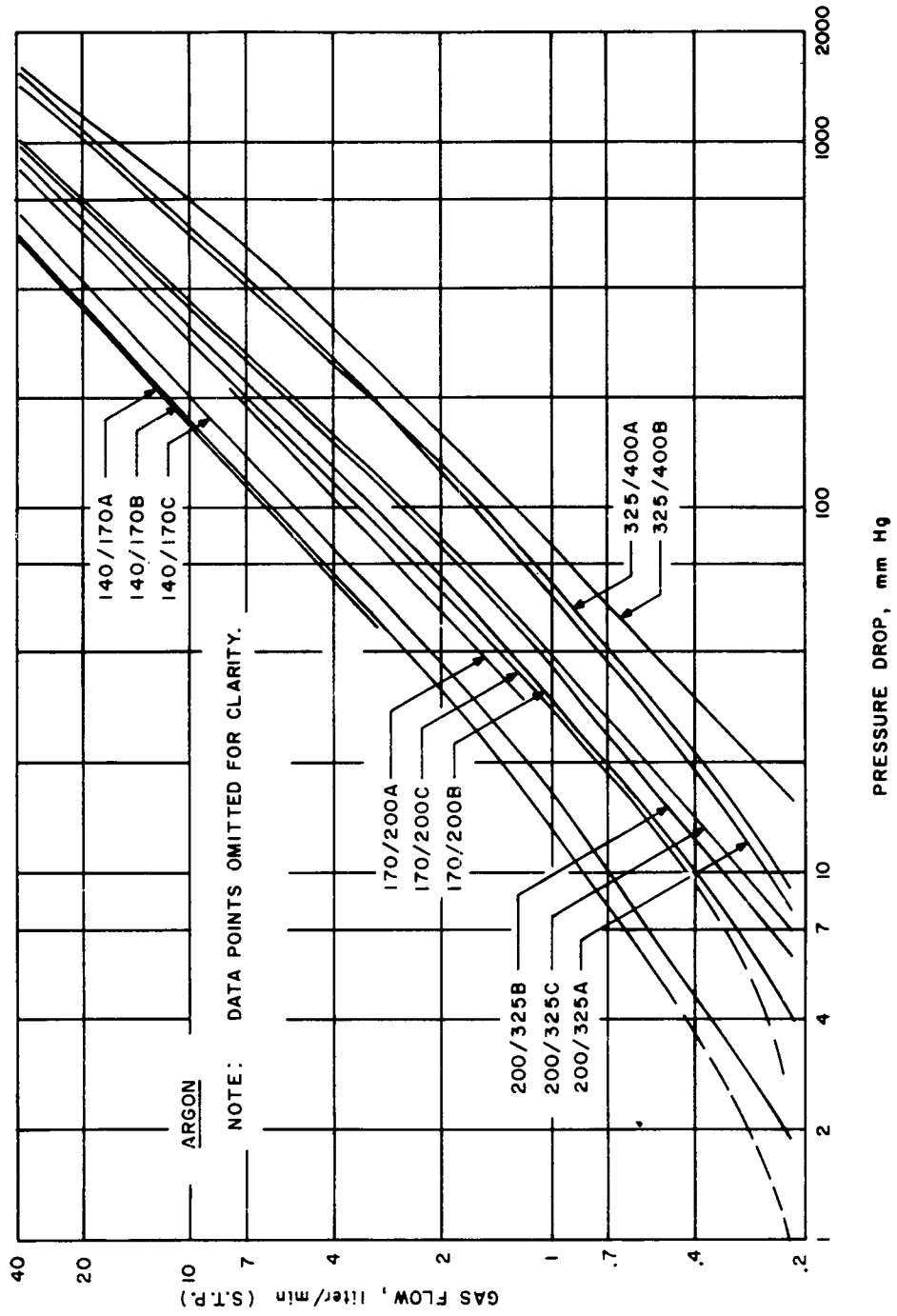


Fig. 5 Gas Flow Rate Plots of Porous Tungsten Specimens for Argon

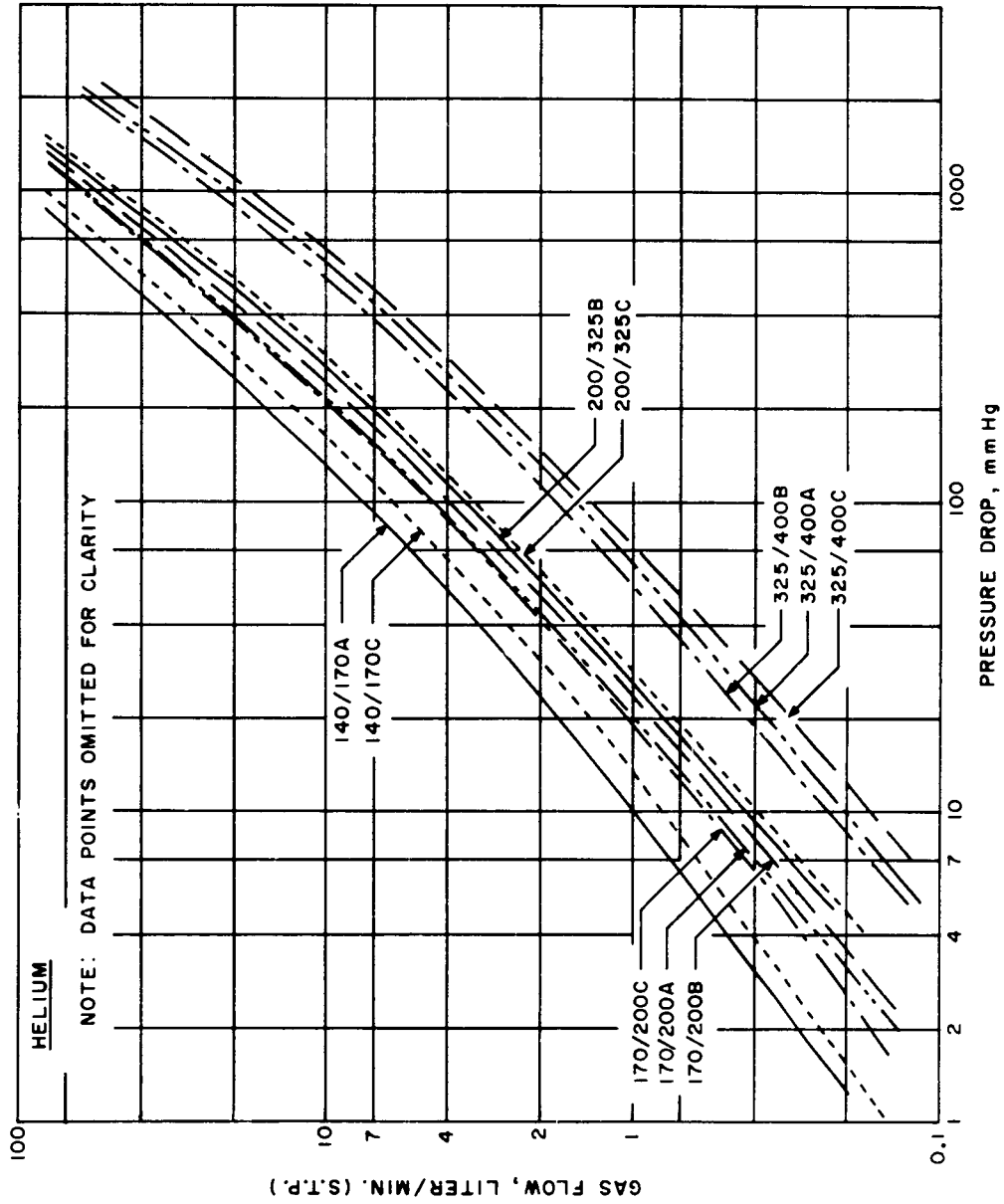
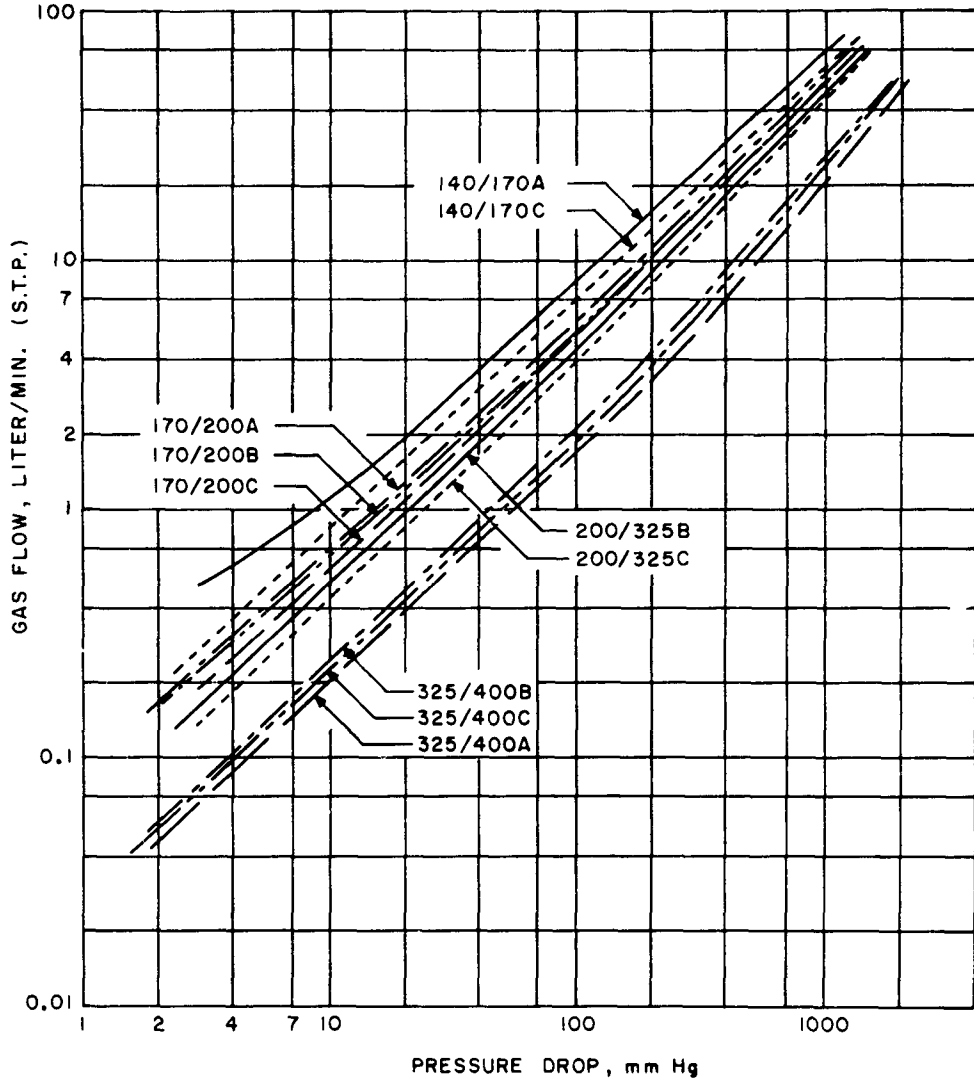


Fig. 6 Gas Flow Rate Plots of Porous Tungsten Specimens for Helium

**NITROGEN**

NOTE: DATA POINTS OMITTED FOR CLARITY



**Fig. 7 Gas Flow Rate Plots of Porous Tungsten Specimens for Nitrogen**

AIR

NOTE: DATA POINTS OMITTED FOR CLARITY

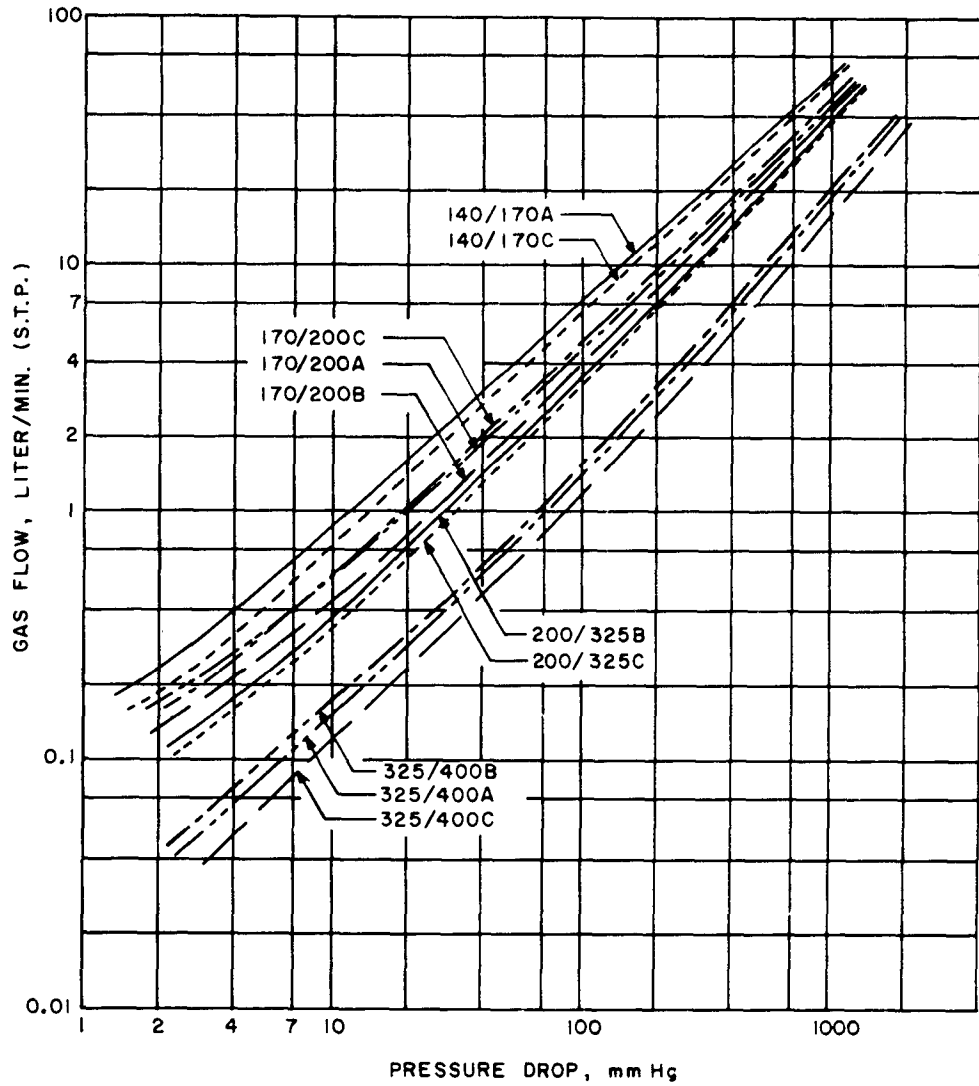


Fig. 8 Gas Flow Rate Plots of Porous Tungsten Specimens for Air

Specimen	Gas			
	Argon	Helium	Nitrogen	Air
140/170A	3.92	5.45	4	3.57
B	3.84	--	--	--
C	3.36	4.56	3.44	3.34
170/200A	2.52	3.25	3.11	2.56
B	2.27	2.94	2.88	2.4
C	2.45	3.25	2.88	2.74
200/325A	--	--	--	--
B	2.04	2.5	2.55	2.05
C	1.96	2.33	2.39	2
325/400A	1.25	1	1	0.96
B	0.94	1.2	1.31	1.05
C	1.04	0.89	1.18	0.8

Fig. 9 Specific Permeability,  $K$ , in  $10^{-8}$   $\text{cm}^2$  for Spheriodized Tungsten Specimens

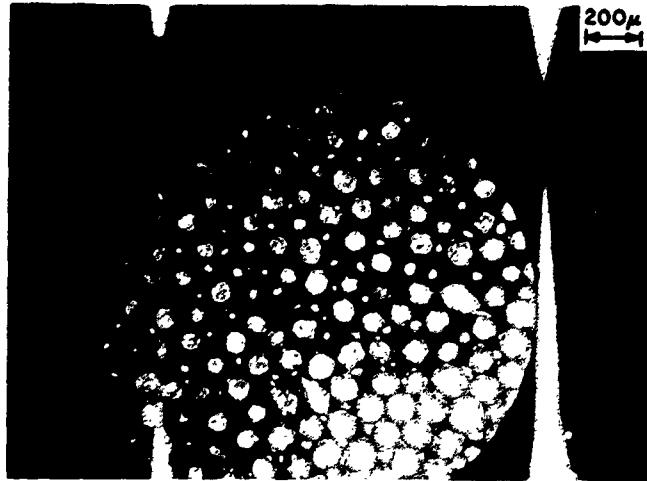


Fig. 10 Photomicrograph: 140/170 Mesh  
Spheroidized Tungsten

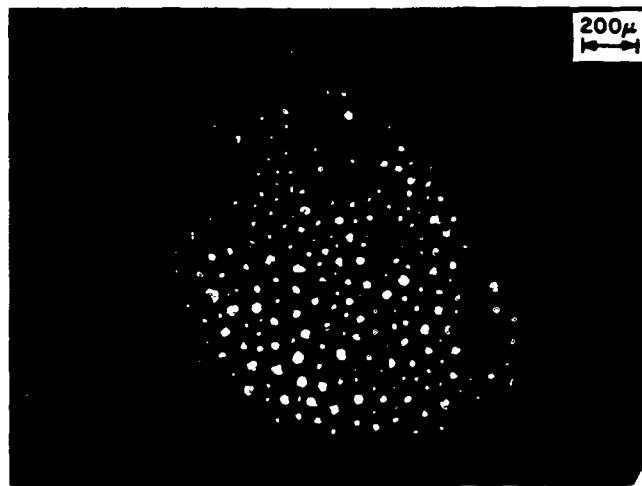


Fig. 11 Photomicrograph: 170/200 Mesh  
Spheroidized Tungsten

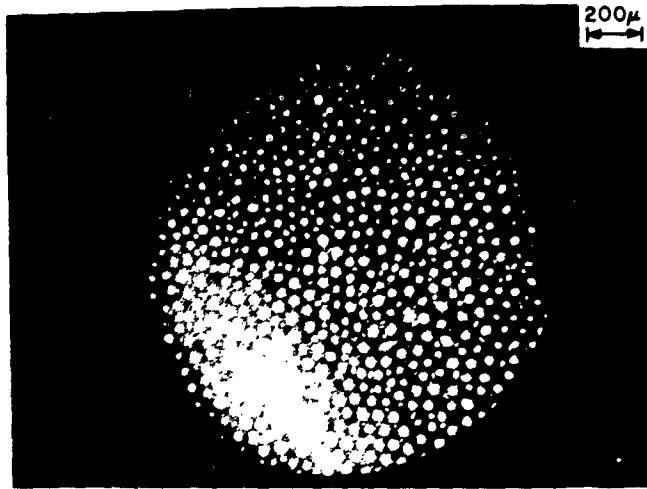


Fig. 12 Photomicrograph: 200/325 Mesh  
Spheroidized Tungsten

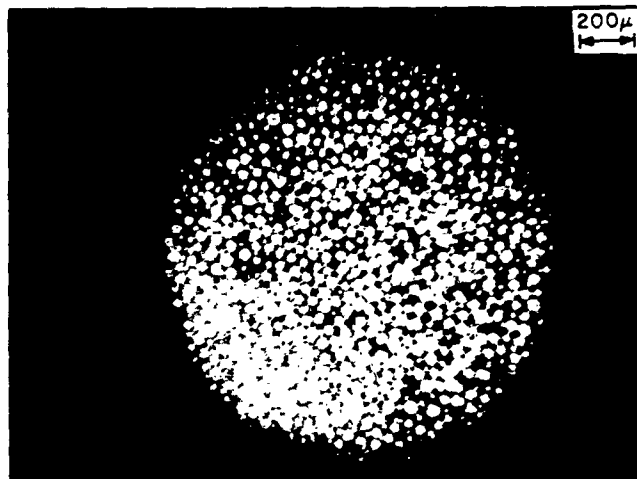


Fig. 13 Photomicrograph: 325/400 Mesh  
Spheroidized Tungsten

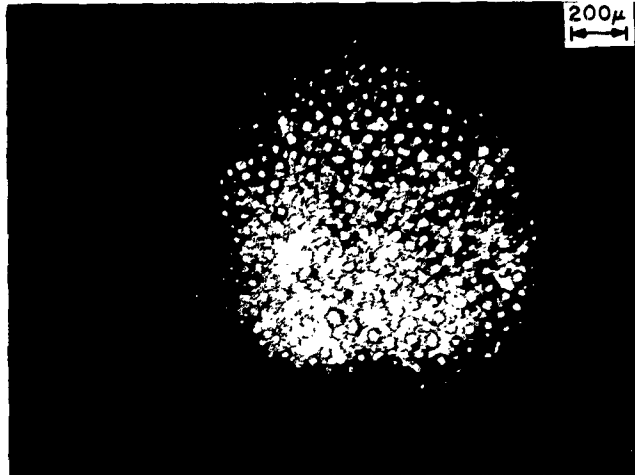


Fig. 14 Photomicrograph: 200/325 Mesh Spheroidized Tungsten  
(Showing plugged area)

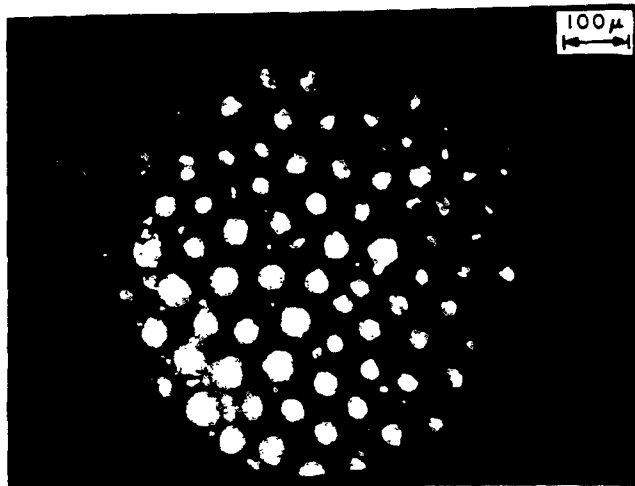


Fig. 15 Photomicrograph: 200/325 Mesh Spheroidized Tungsten  
(Showing plugged area)

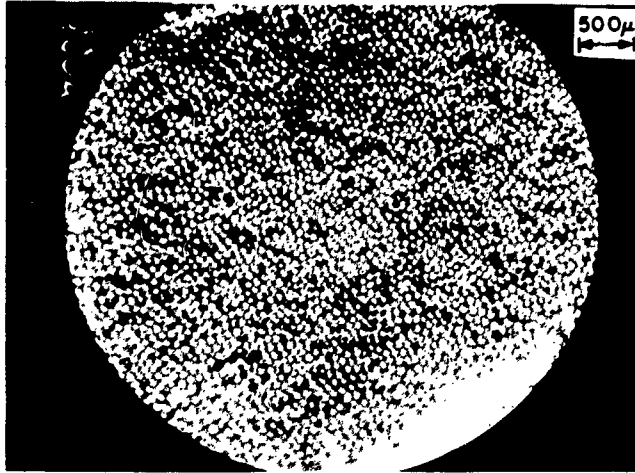


Fig. 16 Photomicrograph: 170/200 Mesh Spheroidized Tungsten  
(Bushing sample)

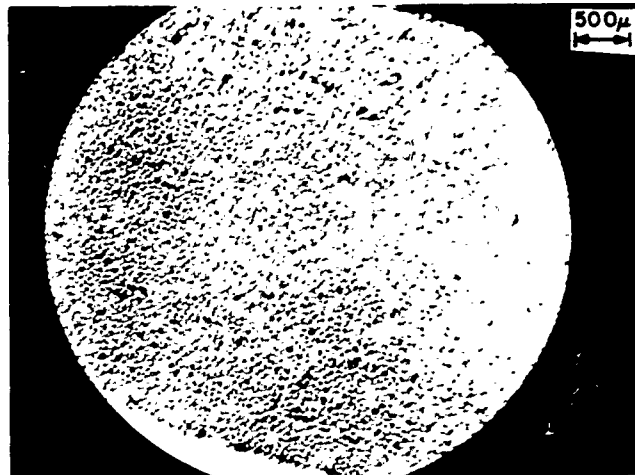


Fig. 17 Photomicrograph: 200/325 Mesh Spheroidized Tungsten  
(Bushing sample)

The mercury penetration results are shown in Figs. 18 and 19 for the 140/170 and 170/200 specimens and indicate average pore size in agreement with the photographs.

Some measured thermal conductivity values are not totally satisfactory. However, later measurements made on a 325/400 specimen at about 95°C and 200°C turned up values of 0.025 and 0.032 cal/sec cm°C, respectively. It is difficult to calculate porous tungsten thermal conductivity from a knowledge of the solid conductivity because of ignorance of the detailed porous structure as well as the bonding. However, extrapolation of the solid conductivity data of Gumenyk and Lebedev<sup>1</sup> shows it to be just about ten times this value. The above comparison is not entirely out of reason since in the spheroidized material contact resistances most likely predominate.

The flow probe of Fig. 3 is only recently put in operation but results made with a crude probe are indicated in Fig. 20. From this figure we can clearly see that large fluctuations dominate the flow pattern. The broken curve in Fig. 20(3) is, with the exception of a peak, indicative of how a good specimen should behave and is to be contrasted with the highly fluctuating curves of other materials indicated in Fig. 20.

## 2. Porous Graphites

In previous work NC-50 and NC-60 have been utilized with some success in fluid transpiration arcs and although it is not expected that these graphites will lead the successful candidates, a certain amount of testing was done on these for comparison.

The flow permeabilities are indicated in Figs. 21 and 22 for air. Comparison with spheroidized tungsten data shows these graphites to be also high in gas permeability. This, of course ensures meeting the first requirement for a satisfactory anode. Figures 23, 24 and 25 are three views of NC-50 with varying magnifications and convey an overall impression of homogeneous spatial distribution of pores although the close-up pictures indicate unsatisfactory macroscopic pore structure, being full of coarse-grained apertures and showing an abundance of pores of the order of 100 to 200 microns. Similar surveys of the NC-60 were also made. Figures 26 to 31 are representative of the surface structures and showing a tolerable over-all picture as in Fig. 28 to very inhomogeneous distributions for most others. The porosimeter determinations are depicted in Figs. 32 and 33. Flow field fluctuations for NC-60 are dramatized in Fig. 20(4) which fully corroborate our photomicrograph studies. The thermal conductivity of NC-60 had been measured to be 0.083 cal/sec cm°C at 90°C and is only about 25 per cent below the extrapolated result of Gumenyk and Lebedev<sup>1</sup> for graphite as well as agreeing approximately with the compilation by Engle and Liggett<sup>2</sup> and National Carbon Co.<sup>3</sup>

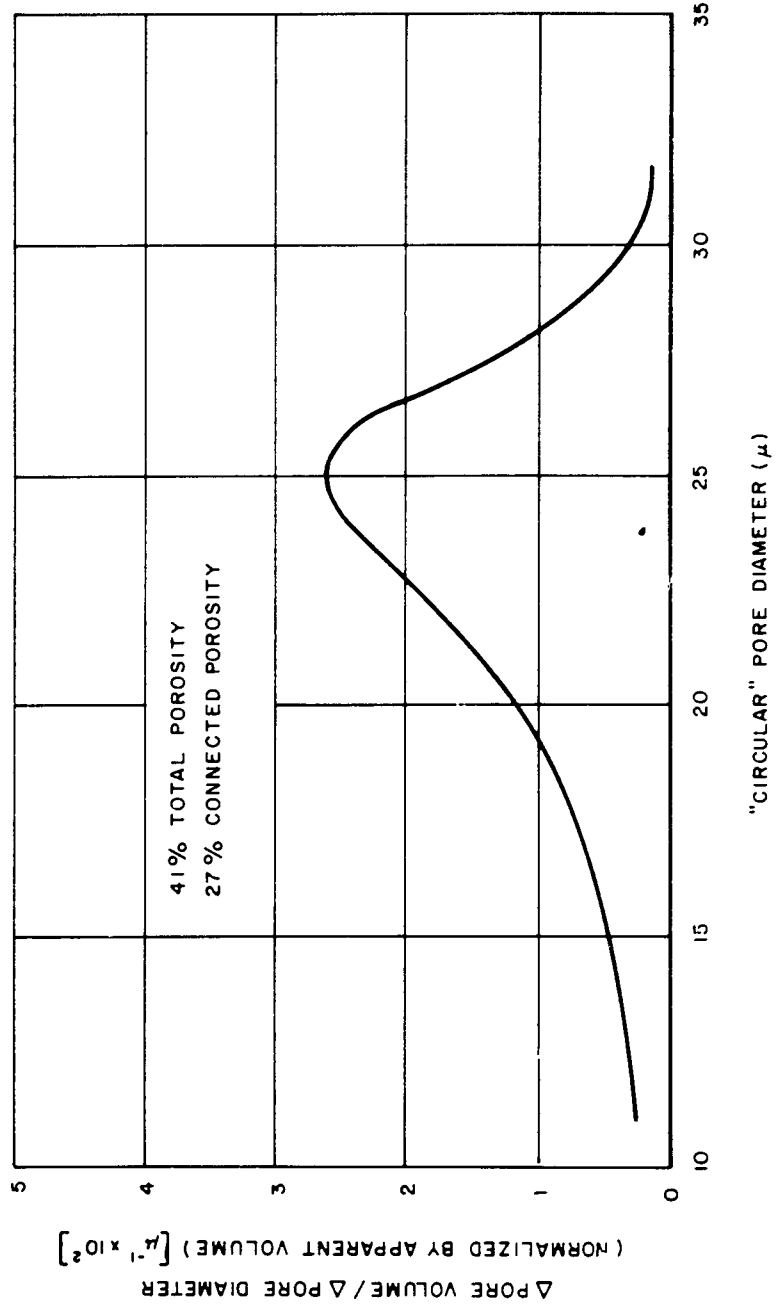


Fig. 18 Pore Size Distribution  
Spheroidized Tungsten (140/170 Mesh)

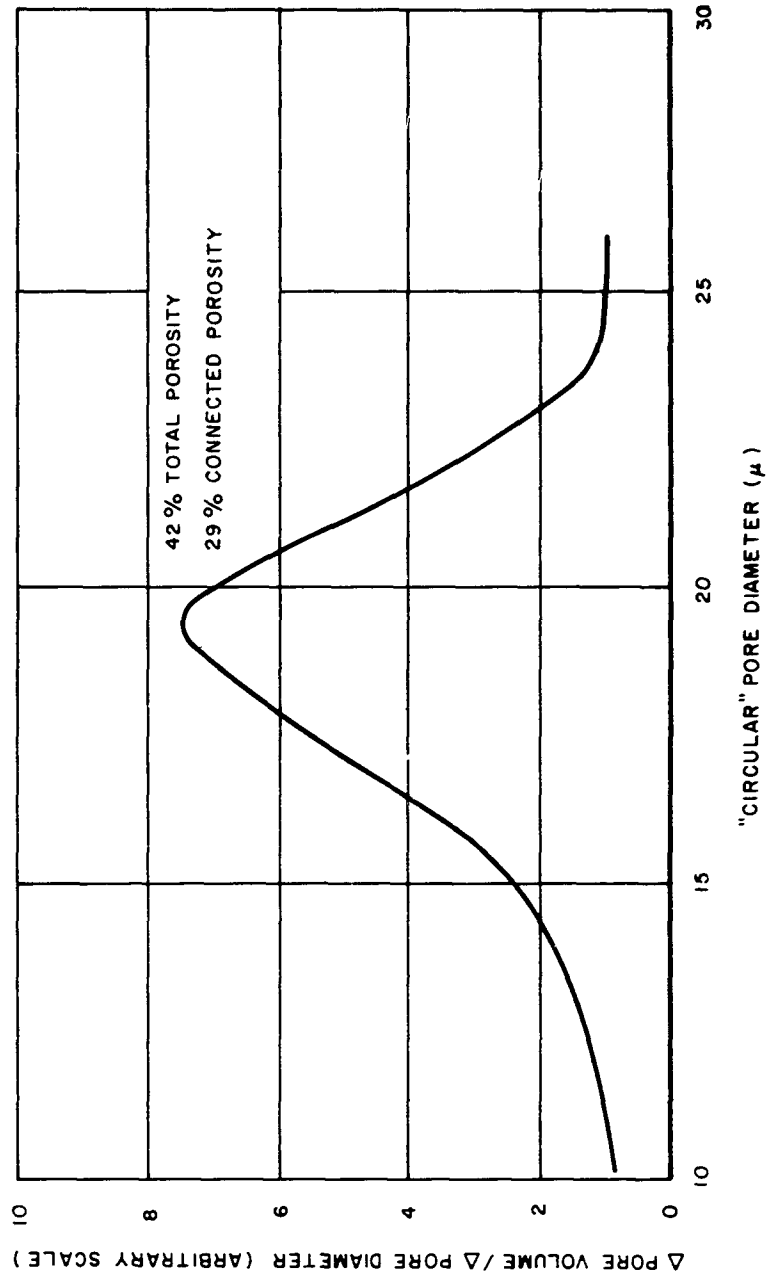
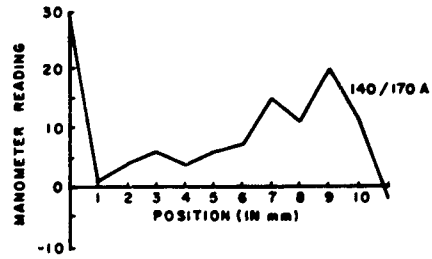
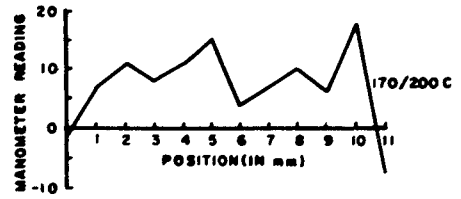


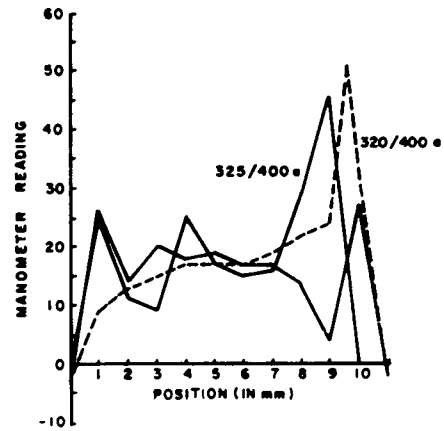
Fig. 19 Pore Size Distribution:  
Spheroidized Tungsten (170/200 Mesh)



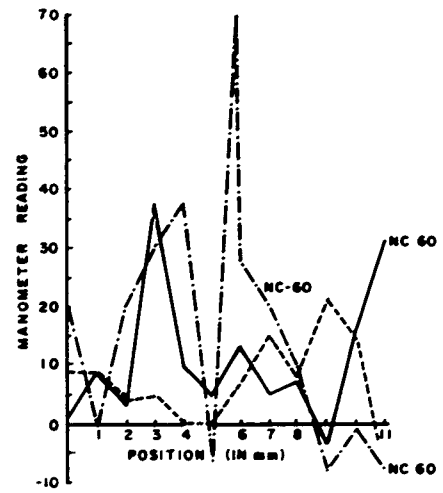
(1) SPHEROIDIZED TUNGSTEN



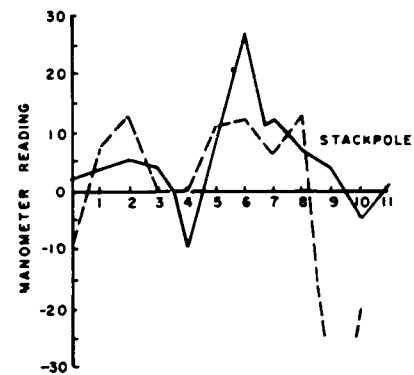
(2) SPHEROIDIZED TUNGSTEN



(3) SPHEROIDIZED TUNGSTEN



(4) GRAPHITE



(5) PC 57

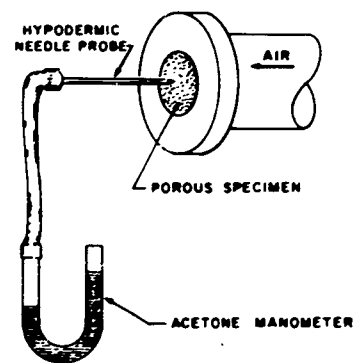


Fig. 20 Local Cold Flow Probe Variation of Porous Specimens

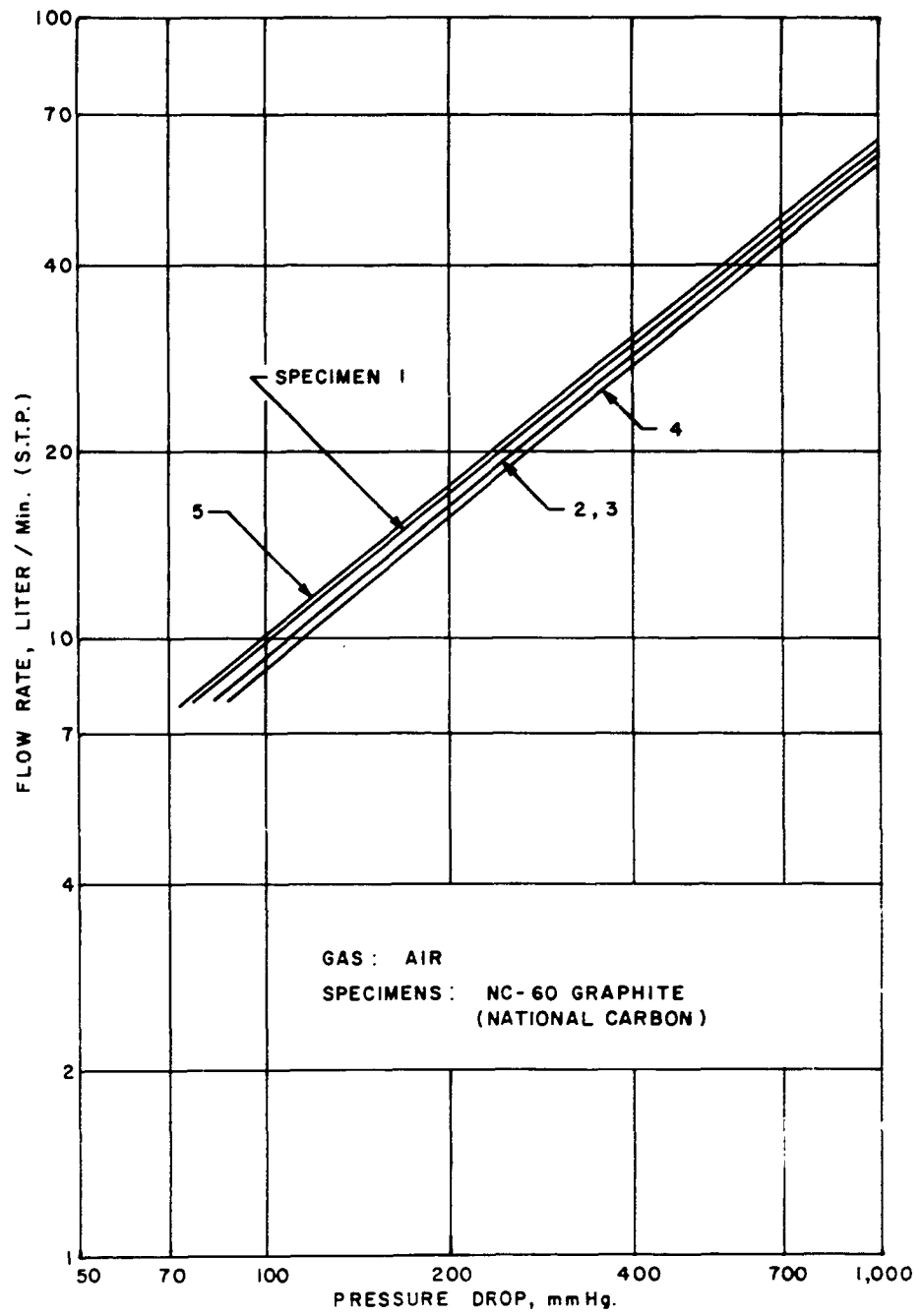


Fig. 21 Gas Flow Rate Plots

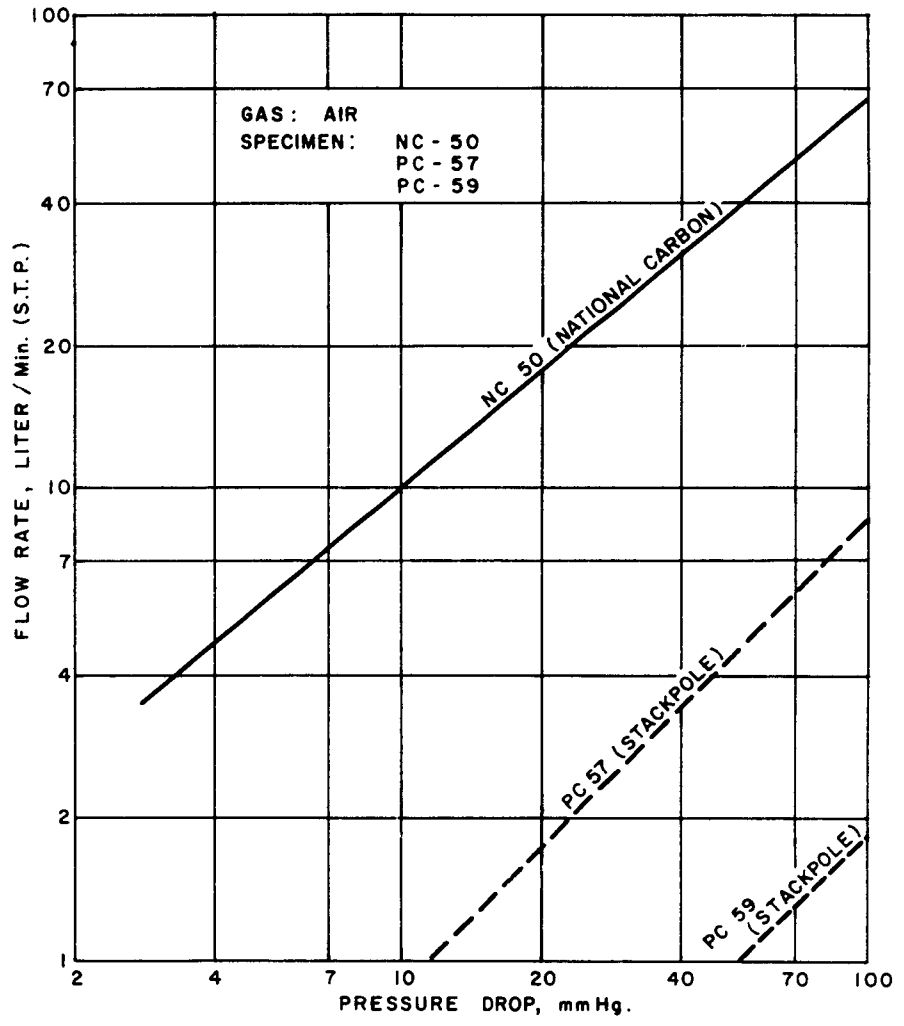


Fig. 22 Gas Flow Rate Plots



Fig. 23 Photomicrograph:

NC 50 Graphite

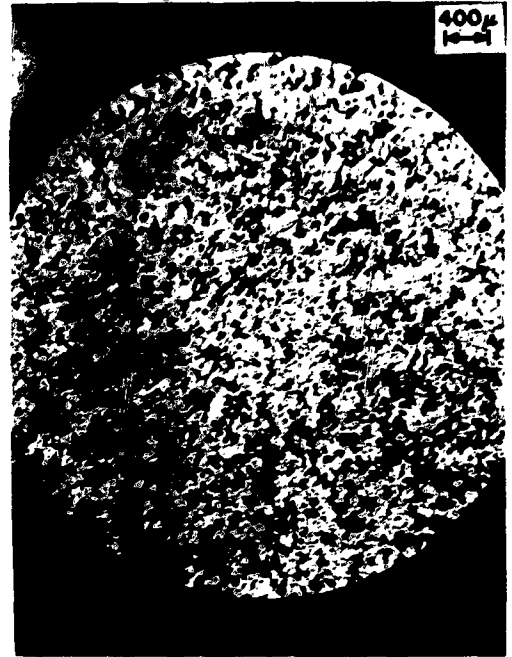


Fig. 24 Photomicrograph:

NC 50 Graphite

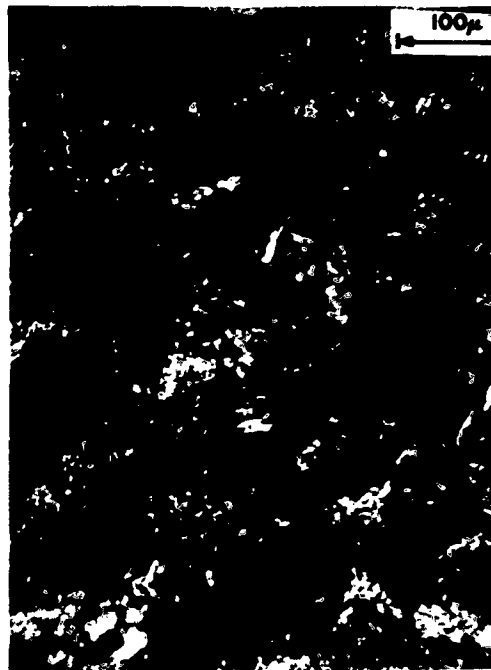


Fig. 25 Photomicrograph:

NC 50 Graphite

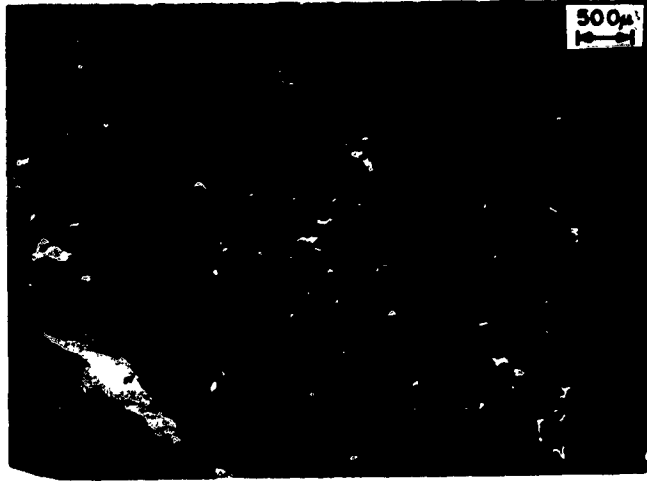


Fig. 26 Photomicrograph: NC 60 Graphite

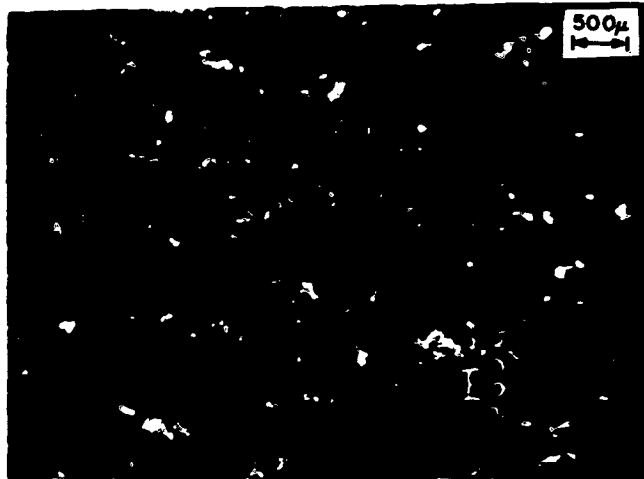


Fig. 27 Photomicrograph: NC 60 Graphite

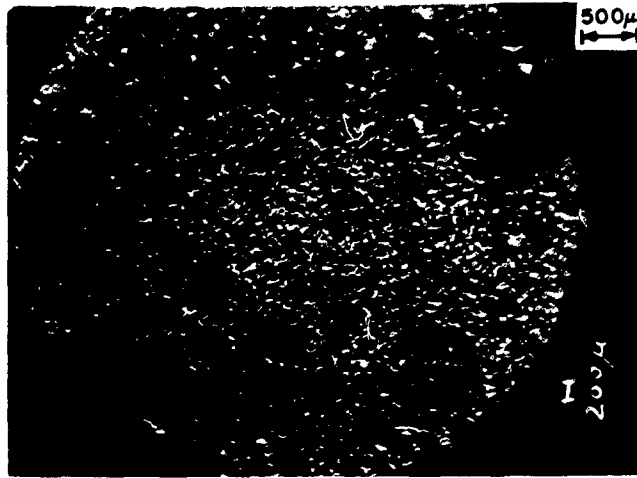


Fig. 28 Photomicrograph: NC 60 Graphite

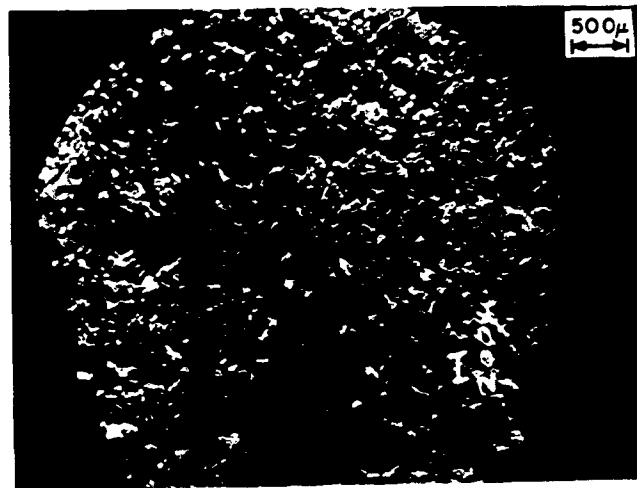


Fig. 29 Photomicrograph: NC 60 Graphite



Fig. 30 Photomicrograph: NC 60 Graphite

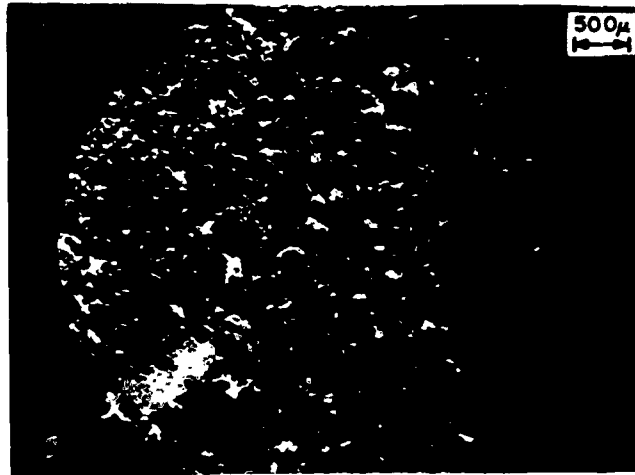


Fig. 31 Photomicrograph: NC 60 Graphite

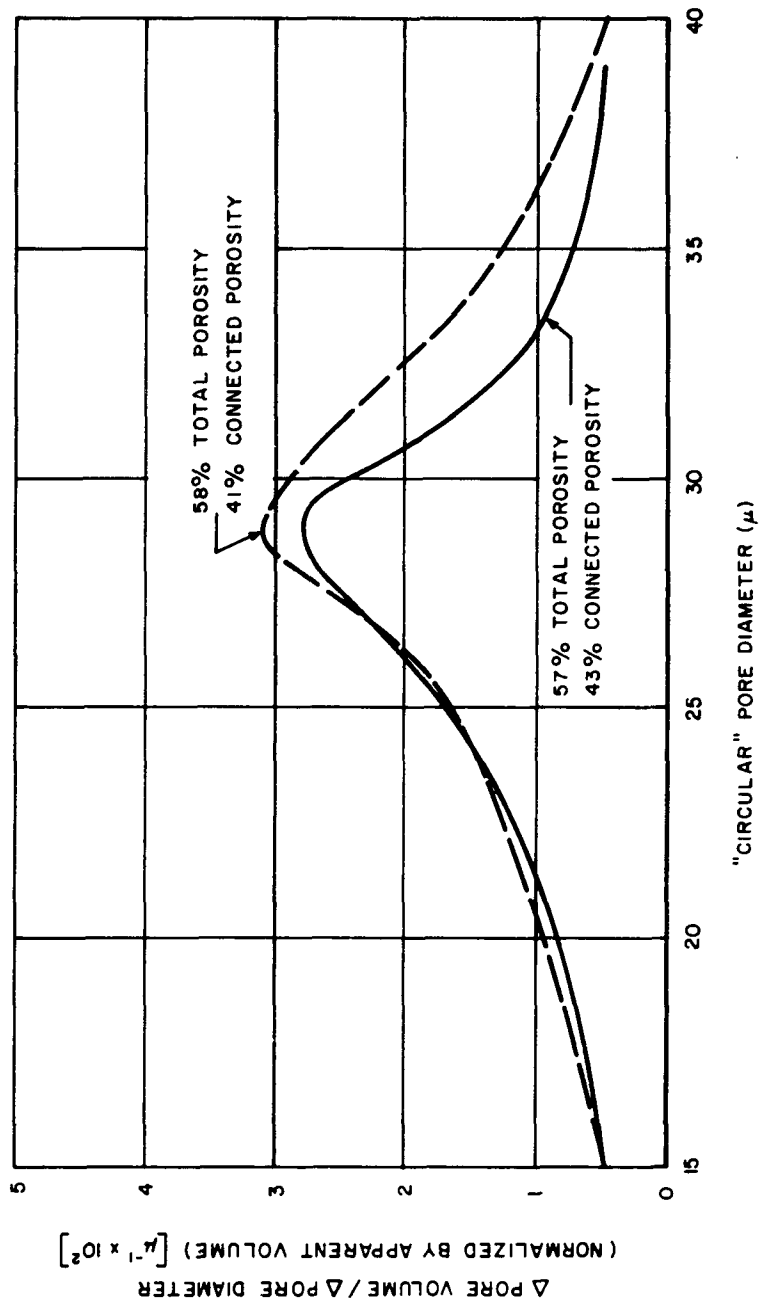


Fig. 32 Pore Size Distribution: NC 50 Graphite

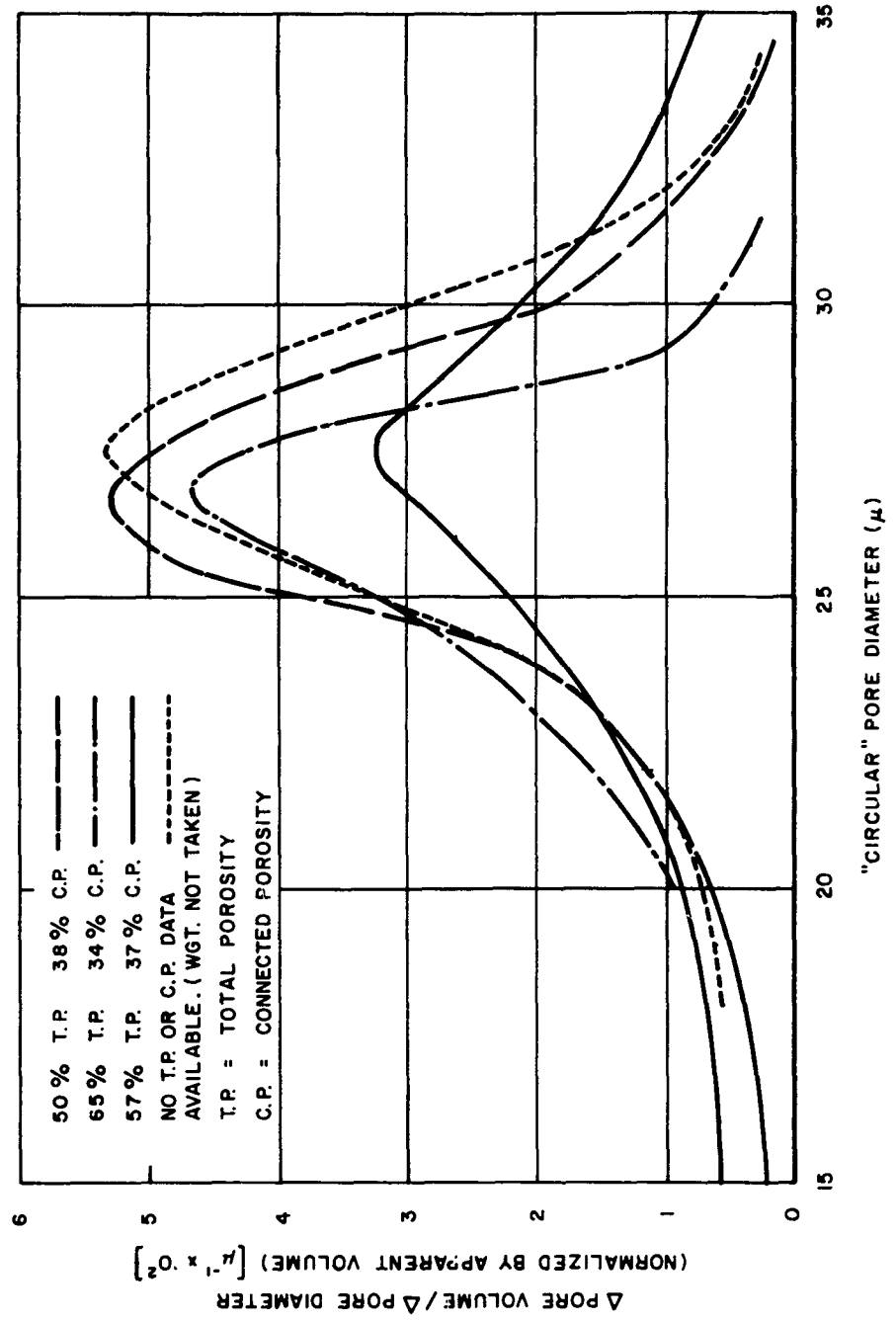


Fig. 33 Pore Size Distribution: NC 60 Graphite

### 3. Stackpole Carbon

The Stackpole PC-57 and PC-59 specimens have been dismissed as being unsuitable to our purposes. The flow permeability data is included in Fig. 22. The extremely low values are obvious. The pore structures appear poor, even by naked eye examination, since isolated deep tunnels are readily detected. Photomicrographic examination for finer details reveals qualities contrary to requirements (see Figs. 34 and 35). The flow nonuniformity as indicated in Fig. 20(5) is, therefore, to be expected. The thermal conductivity indication is also poor, being one order of magnitude below that for NC-60.

### 4. Huyck Feltmetal

Feltmetal is the latest material to be evaluated by us. It is manufactured with porosities ranging from 40 to 90 per cent and is available in different metals including stainless steel and tungsten. The flow permeability data supplied by the Huyck Corporation indicate promise. Some Feltmetal photomicrographs are shown as Figs. 36 and 37. Since these are 90 per cent porous samples the feltlike appearance is understandable and does not seem to conform to our criteria. However, the less porous grades may yet prove suitable for our use; these are currently being tested. A curve from the Porosimeter determination is included in Fig. 38, both the distribution and the porosity figures are in good agreement with Huyck data.

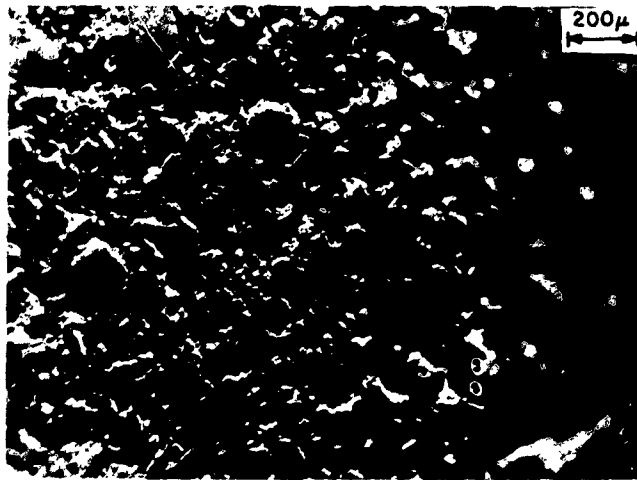


Fig. 34 Photomicrograph: PC-57

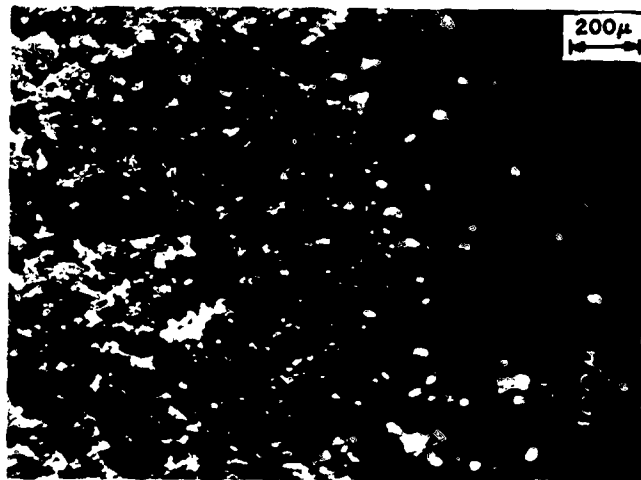


Fig. 35 Photomicrograph: PC-59

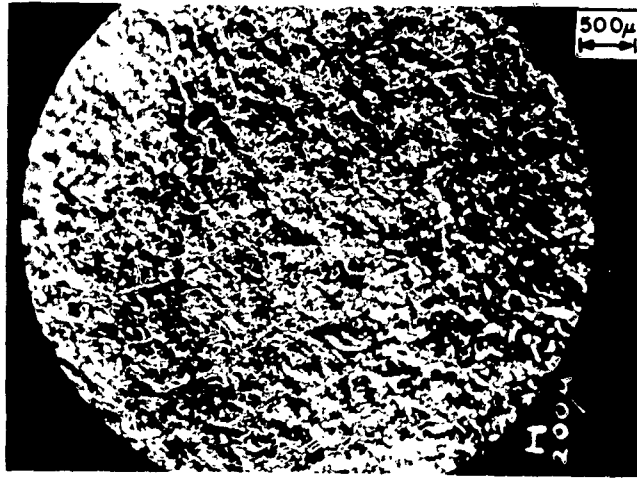


Fig. 36 Photomicrograph: Feltmetal 90 Per Cent Porosity Type A Fiber, 302 Stainless Steel

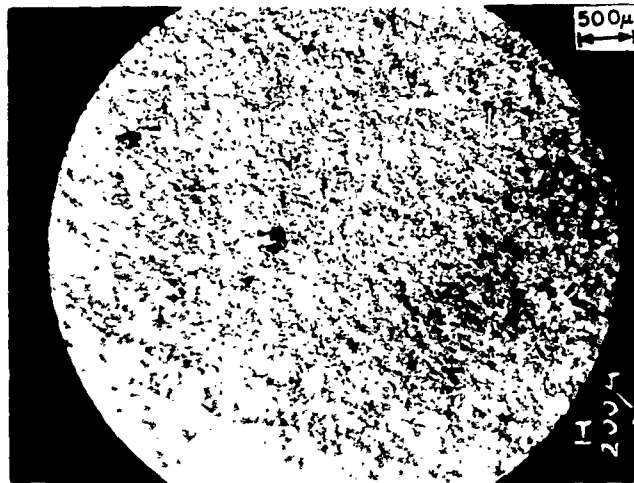
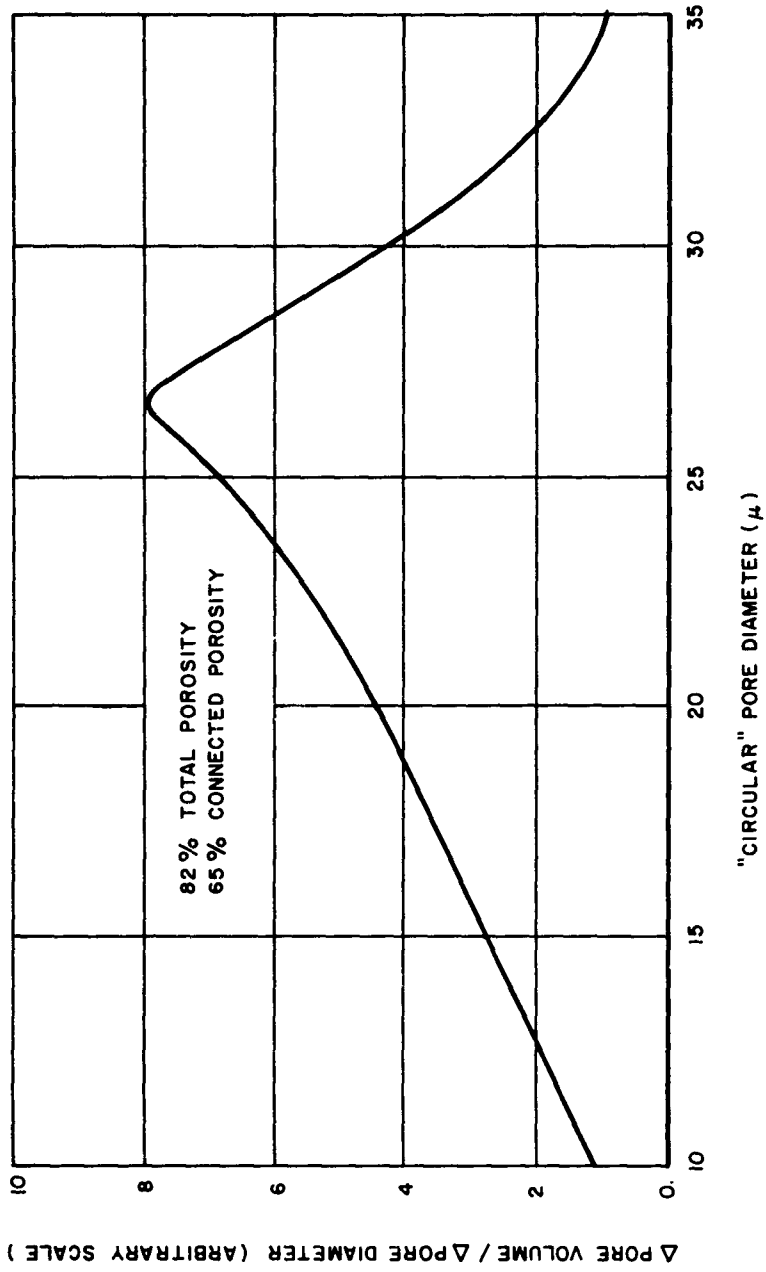


Fig. 37 Photomicrograph: Feltmetal 90 Per Cent Porosity Type A Fiber, 302 Stainless Steel



**Fig. 38 Pore Size Distribution:  
Feltmetal 90 Per cent Porosity Type A Fiber, 302 Stainless Steel**

### III. ARC ASSEMBLY DEVELOPMENT

#### A. GEOMETRY OF THE ARC ASSEMBLY: THE TRIPLE CATHODE GEOMETRY

If the thermal, mechanical and electrical properties of a porous anode are to be related to the performance of the anode in a fluid transpiration arc, then the geometry of the arc assembly must be simple enough to admit of analytical attack. This requires as high a degree of symmetry in the electrode geometry as is consistent with the mechanical requirements of construction. Since this study is concerned primarily with phenomena in the anode sheath and transition regions, it is especially important to maintain symmetry in the vicinity of the anode. If spherical symmetry is ruled out for mechanical reasons, then cylindrical symmetry becomes attractive. To achieve cylindrical symmetry, one electrode can be located on the cylindrical axis facing axially while the other electrode is located at some radius from the axis. The simplest and most symmetrical geometry of this type would consist of a central disk electrode and a second annular electrode which need not be coplanar. However, early experiments with this geometry<sup>4</sup> show a strong tendency for the arc to strike to a single location on the annular electrode rather than to distribute its termination around the entire annulus. This destroys the symmetry and is hence undesirable. However, the simple geometry may be approximated by disposing several electrodes with an equal azimuthal spacing in place of the annular electrode. By mechanical adjustment and electrical ballasting of the several electrodes the arc may be maintained with approximately equal current flow to each. Symmetry dictates as many such electrodes as possible, while mechanical convenience argues for as few as possible. Three such electrodes were decided upon in this study as being the smallest number to give a reasonable degree of symmetry. The anode was chosen to be the central electrode. Thus the geometry of the arc assembly for this study consists of a central disk-shaped anode surrounded by three cathodes with a 120-deg azimuthal spacing.

It is desirable in operating the arc to vary both the anode-cathode distance (arc gap) and the position of the plane containing the cathode with respect to the plane of the anode surface. The interesting possibility involving the latter variation is shown in Fig. 39. In this sketch the cathode plane is located behind the anode plane so that the cathode jets flow in the same direction as the gas transpired through the anode surface. This arrangement should minimize or eliminate turbulent interaction between the cathode jets and the transpired gas flow and at the same time preserve the cylindrical symmetry in the vicinity of the anode as called for in the contract statement of work. This geometry will therefore simplify the analytical approach to the problem and facilitate access to the arc flame for spectroscopic and probe diagnostics. It would, however, be difficult or impossible to strike the arc with this electrode geometry. Hence operation in this mode requires simultaneous motion of the three cathodes and/or the anode while the arc is running. A typical operating sequence is shown in Fig. 40. The arc is struck with the three cathodes close to and in front of the

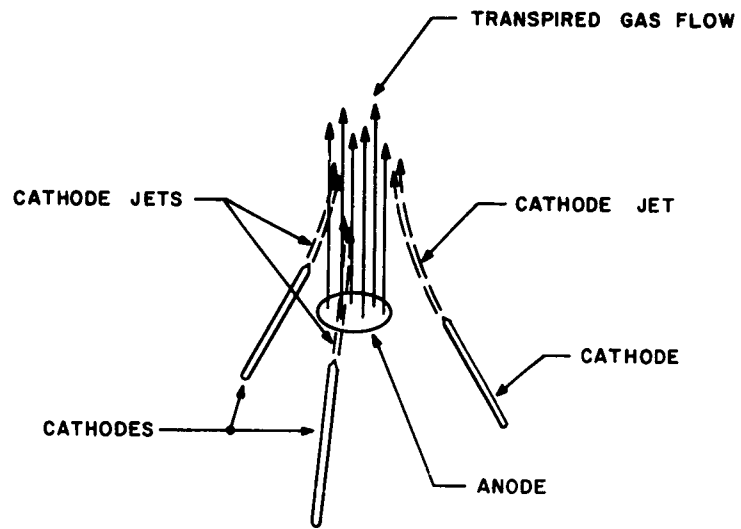


**Fig. 39** Geometry of Cathode Jets and Transpired Gas Flow with Cathodes in Swept Back Position

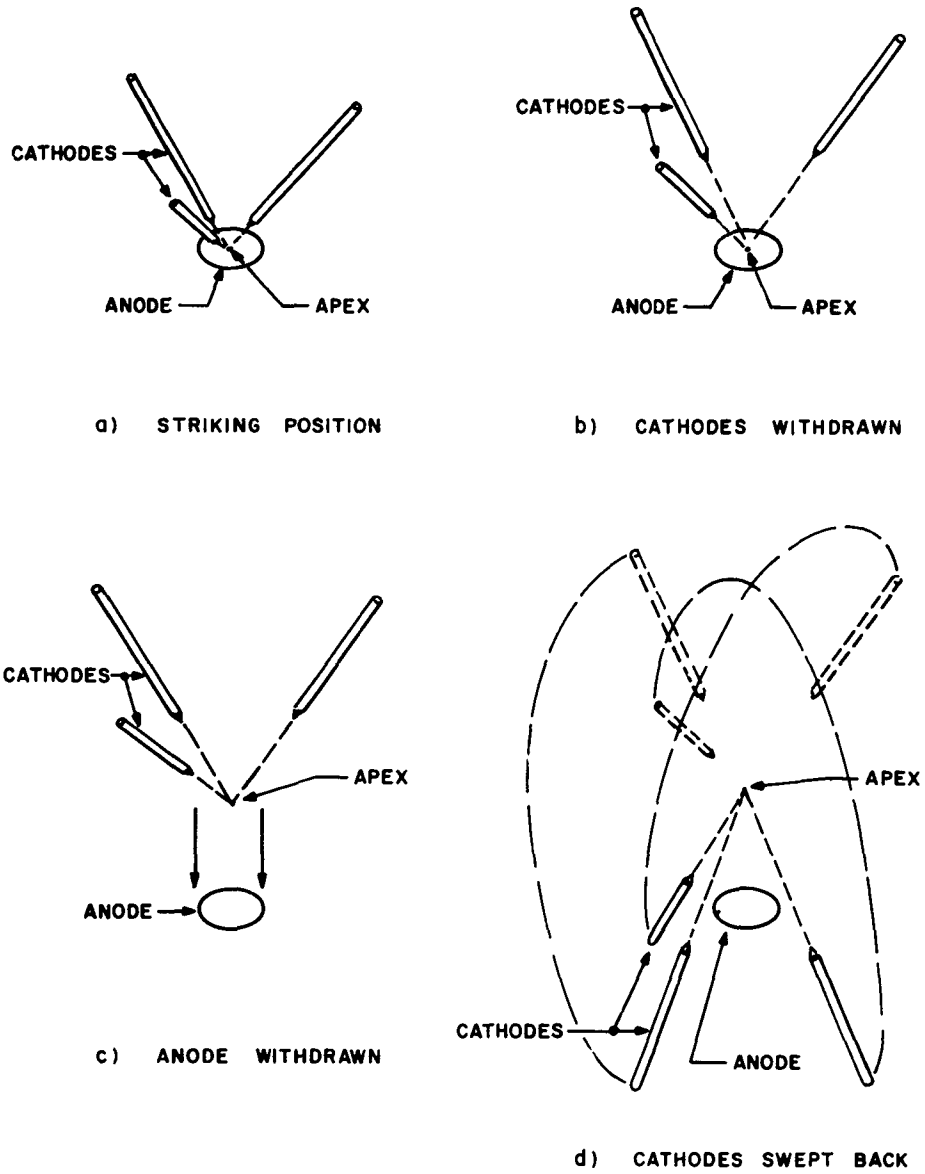


Fig. 40 Typical Operation of Triple Cathode Arc Assembly

anode (Fig. 40a). Then the cathodes and anodes are withdrawn (Fig. 40b and 40c). Finally the cathodes are simultaneously swept back behind the anode (Fig. 40d) to achieve the geometry of Fig. 39.

#### B. DESIGN OF THE ARC ASSEMBLY

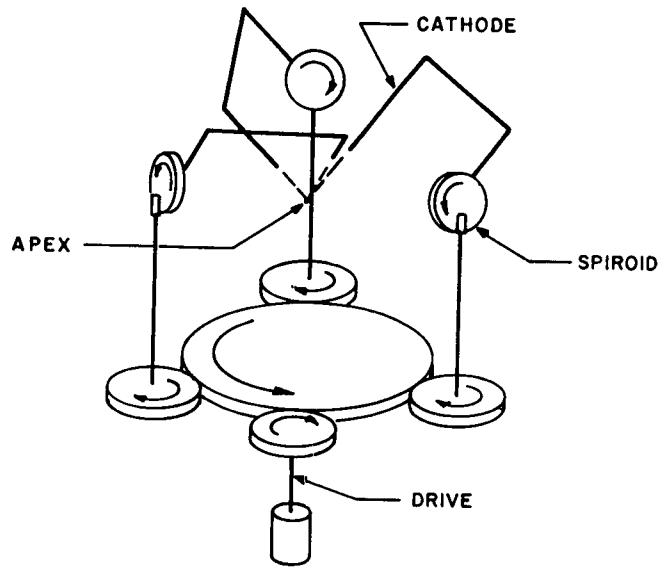
Since these operations must be effected without destroying the symmetry of the arc considerable precision is required in the arc assembly. Since both linear and angular motion of the cathodes is required while the arc is running, the assembly design is much more complicated than the conventional collinear geometry. Fig. 41 shows the adopted solution to these two problems of cathode motion. In Fig. 41a the angular motion of the cathode is depicted. A large central gear is driven from a motor by a driver gear. Shafts, attached to three identical spur gears and driven from the central gear, drive in turn three spiroid gears. The axes of rotation of the three spiroid gears are coplanar and meet on the axis of symmetry on the assembly in a point called the apex. The rod-shaped cathodes, rigidly attached to the spiroid gears, are thus caused to rotate symmetrically about the apex and the plane containing the cathode tips is displaced axially with respect to the apex while symmetry is maintained. In Fig. 41b the linear motion of the cathodes is depicted. The driving arrangement is similar to the previous case but bevel and worm gears replace the spiroid gears and cause a threaded rod to which the cathodes are attached to move toward or away from the apex. The anode motion (not shown) is a simple axial translation toward or away from the apex driven by a third motor.

The linear travels of the anode and the three cathodes are three inches with a design tolerance of 0.010 inch. The angular design tolerance is 0.002 radians. Angular travel is restricted in the forward position by the interference of the cathodes with each other and in the swept-back position by the interference of the cathodes with the anode. In each position it is possible to move the cathodes to within ten to twenty degrees of the axis.

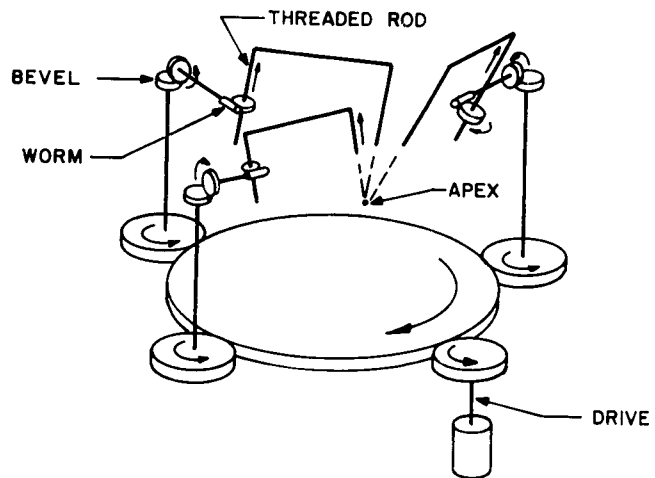
Figure 42 is an assembly drawing of the anode and one of the cathode arms and indicates the complexity of the design necessitated by the required precision and simultaneity of the several movements during arc operation.

#### C. PROGRESS TO DATE IN THE FABRICATION OF THE ARC ASSEMBLY

Figure 43 is a photograph of the machined parts which comprise the triple cathode arc assembly. Figure 44a shows the major parts which comprise the anode structure. Figure 44c shows the major parts for one of the cathode arms. Figure 44b shows the major parts for the baseplate sub-assembly on which the anode and cathode structures are mounted and which in its turn is mounted in the arc chamber. Assembly of this unit together with a support structure, provision of gas, electrical and water services and provision of thermal and electrical protection is now in progress. Complete assembly is anticipated by June 1, 1963.



a) ANGULAR CATHODE MOTION



b) LINEAR CATHODE MOTION

Fig. 41 Cathode Motion

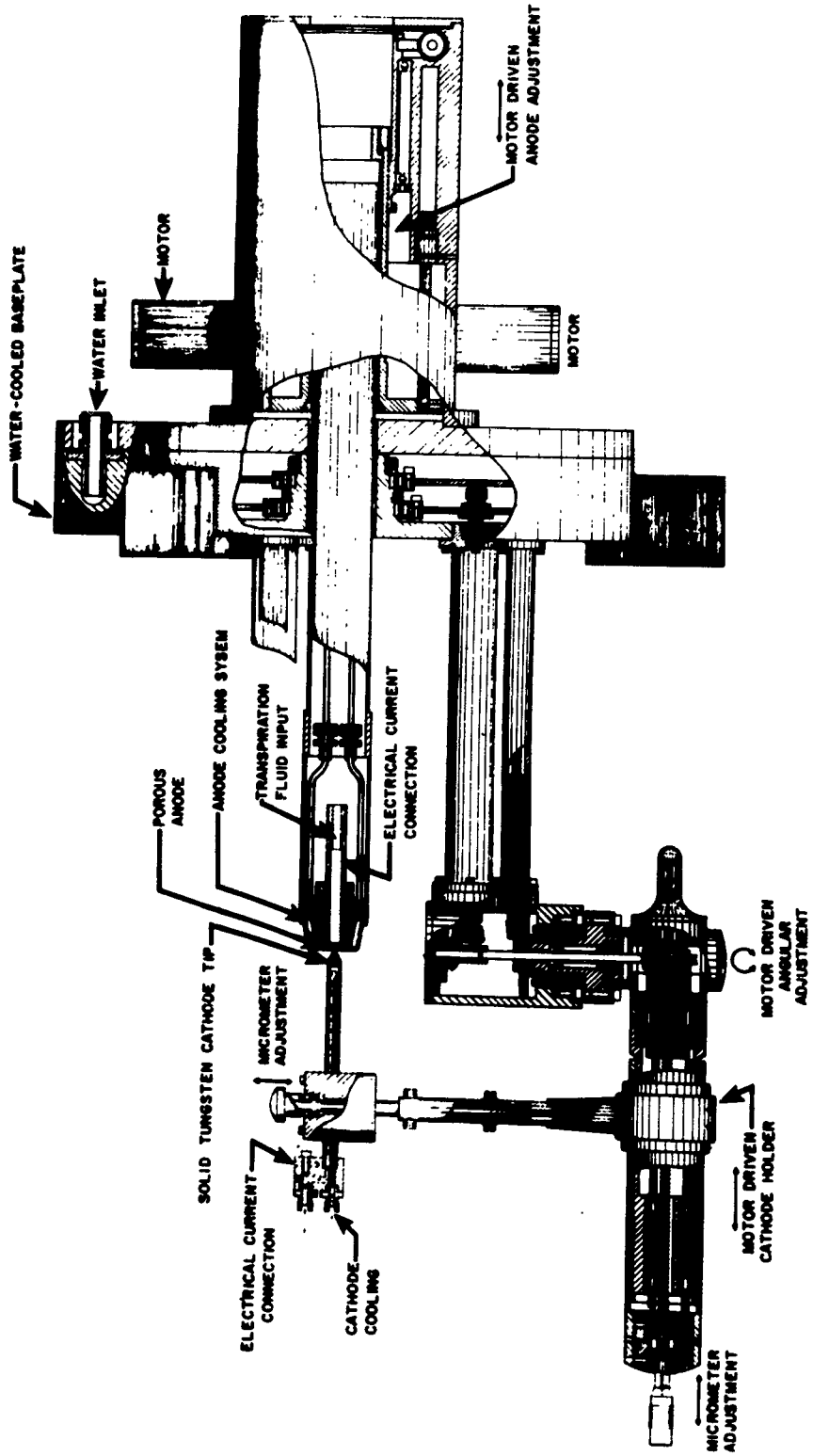


Fig. 42 Triple-Cathode Arc Assembly (Showing one of the three cathode mechanisms)

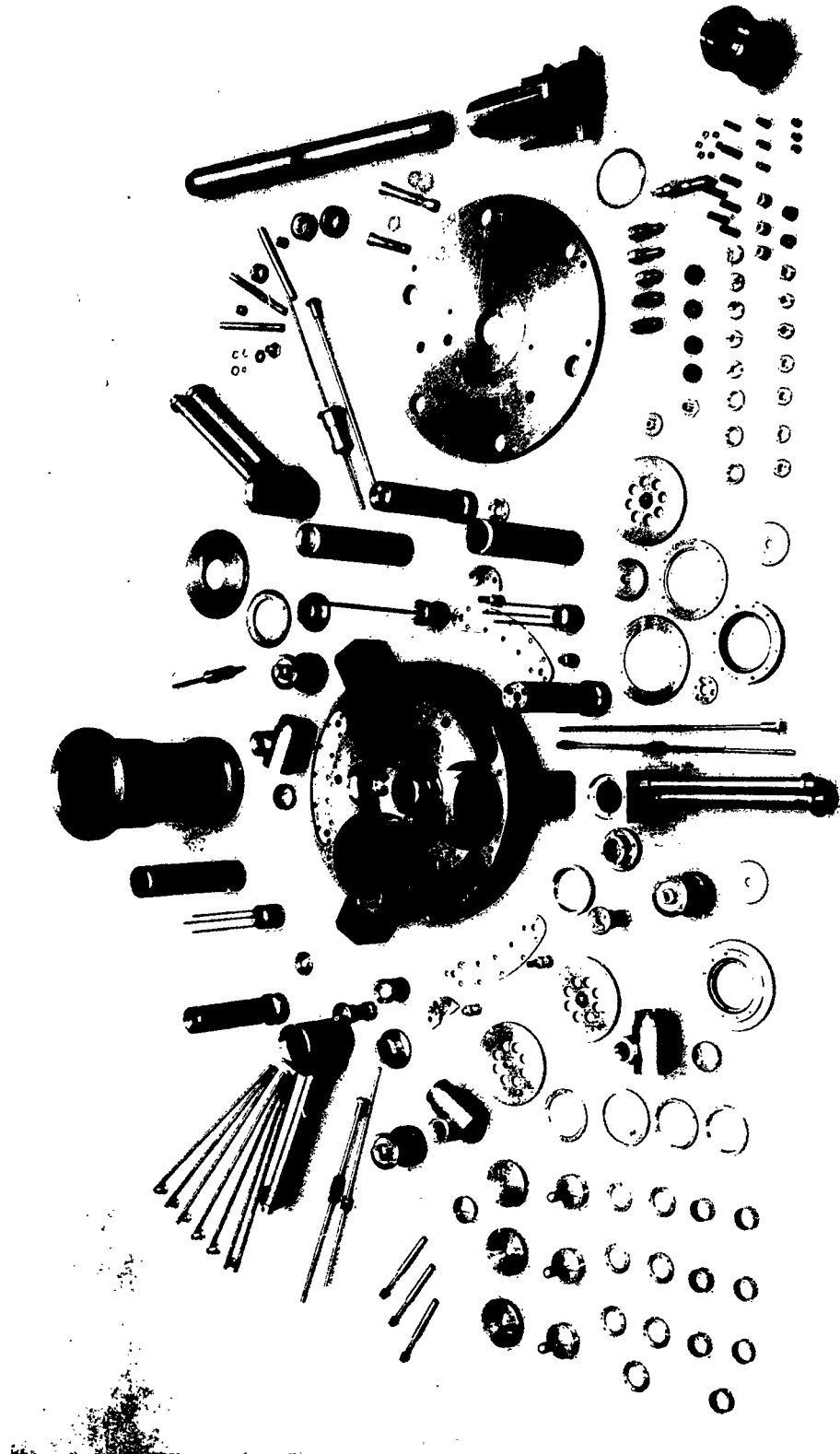
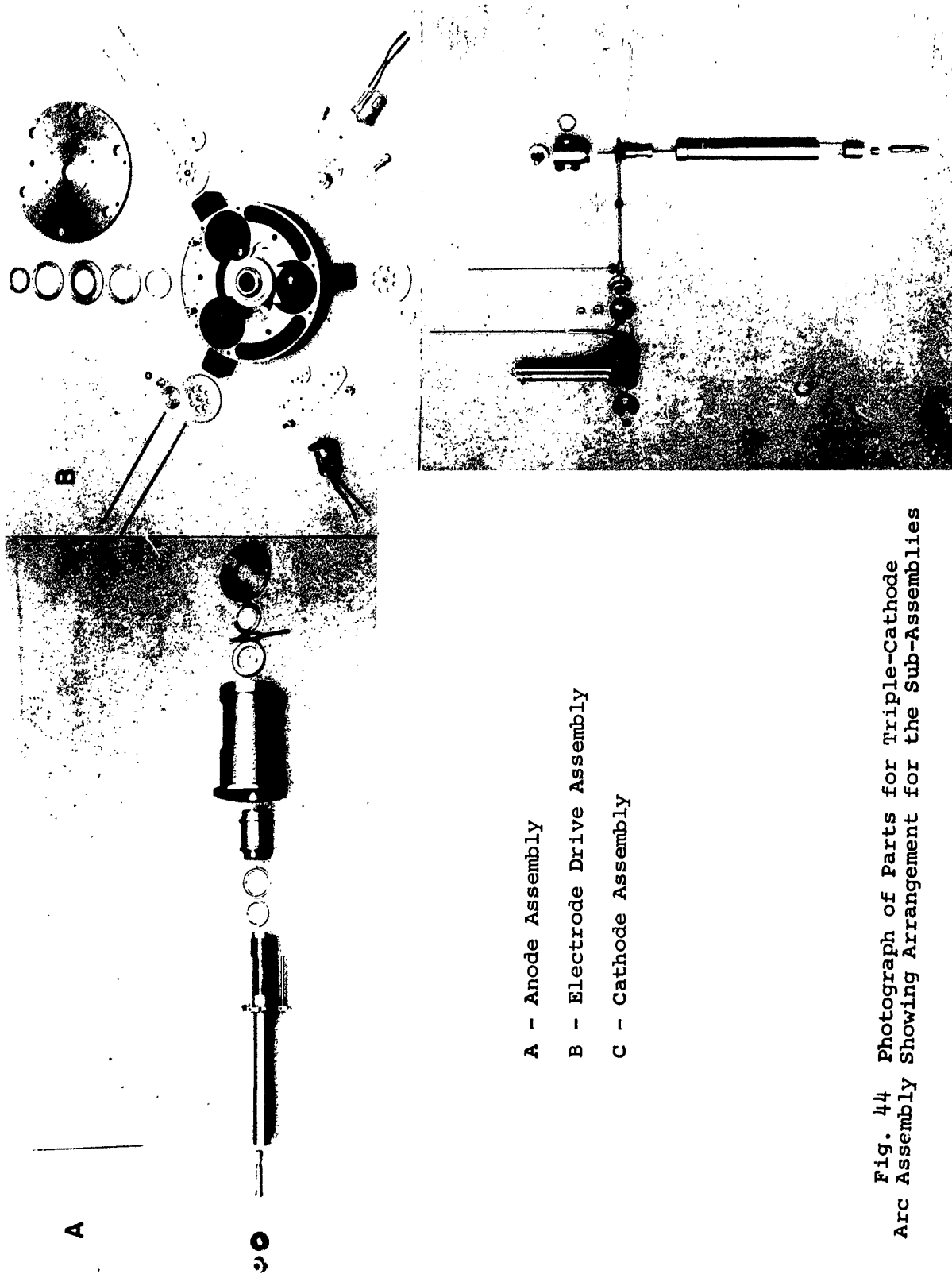


Fig. 43 Photograph of Parts for Triple-Cathode  
Arc Assembly



- A - Anode Assembly
- B - Electrode Drive Assembly
- C - Cathode Assembly

Fig. 44 Photograph of Parts for Triple-Cathode Arc Assembly Showing Arrangement for the Sub-Assemblies

#### D. INTERIM ARC ASSEMBLY

The long fabrication time dictated by the complexity and precision of the triple cathode arc assembly described above made it desirable to make some preliminary tests of anode materials in a simpler arc assembly. Several versions of such an assembly were employed, having in common the features sketched in Fig. 45. A central conical tungsten cathode is mounted on a copper tube which supplies cooling water and electrical service and separated by a 1/16" boron nitride insulator from a 1/16" annular anode surface. Transpiration gas is introduced from the rear or side of the porous anode. The several versions differed in the methods of gas introduction and anode water-cooling, water and gas sealing and mechanical mounting of the various parts.

This geometry was chosen because some success was achieved in previous experience with this arrangement.<sup>4</sup> The experiments conducted in this study were necessarily qualitative but they did permit some conclusions to be drawn.

A persistent tendency for the arc to strike to terminate asymmetrically instead of spreading uniformly around the annular anode characterized these preliminary experiments. In experiments with porous carbon anodes (NC 60) local flow probe measurements similar to those described in Sec. II-C above indicated considerable inhomogeneity in the transpired gas flow in the absence of the arc. This led to the photomicrographic survey of a large number of porous carbon samples which survey is described in Sec. II-C. As reported there this survey indicated a very great degree of inhomogeneity in the structure of the porous carbon material and raised grave doubts as to the suitability of this material for anodes in a transpiration arc.

It was expected that sintered spheroidized tungsten anodes would exhibit a greater degree of uniformity of structure than did the porous carbon. Photomicrographs and local flow probe measurements described in Sec. II-C confirmed this expectation and one attempt was made to use this material in the simplified arc assembly shown in Fig. 46. The tungsten anode bushing was copper-plated on all exposed surfaces except for the annular anode face at the front and a similar annular surface at the rear through which the transpiration gas was introduced. The plated copper provided a gas seal around the anode and good thermal and electrical conductivity to the support structure. In addition, the available copper surface at the rear of the anode made it possible to braze or solder the anode to its support, greatly simplifying the assembly. Soft solder was used in this case to avoid oxidizing the tungsten and reducing the heat transfer coefficient but brazing could be accomplished in an inert or reducing atmosphere. Local flow probe measurement of the transpired gas flow in the absence of the arc yielded the results shown in Fig. 47. The salient feature of this curve is the concentration of the gas flow in the azimuthal region from 180° to 360° and the apparent lack of gas flow in the region around 110°. When struck, the arc seemed from visual observations to concentrate in this latter region. This simple experiment is taken as confirmation of the need for a homogeneous anode material.

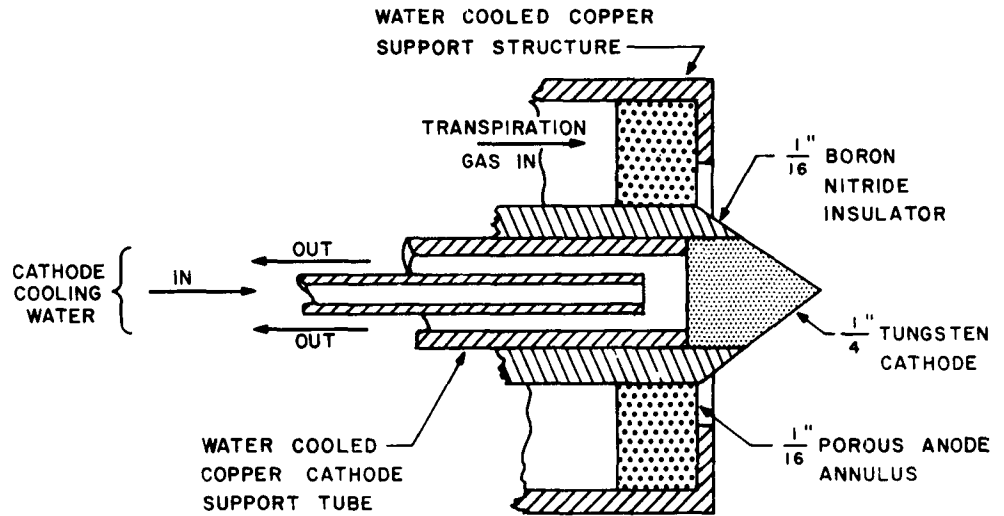
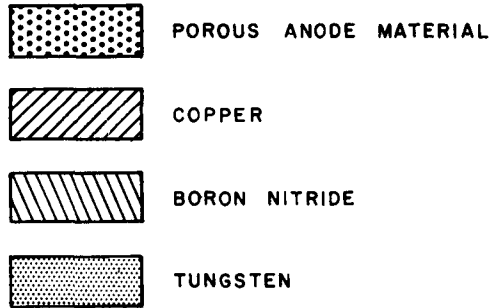


Fig. 45 Interim Arc Assembly

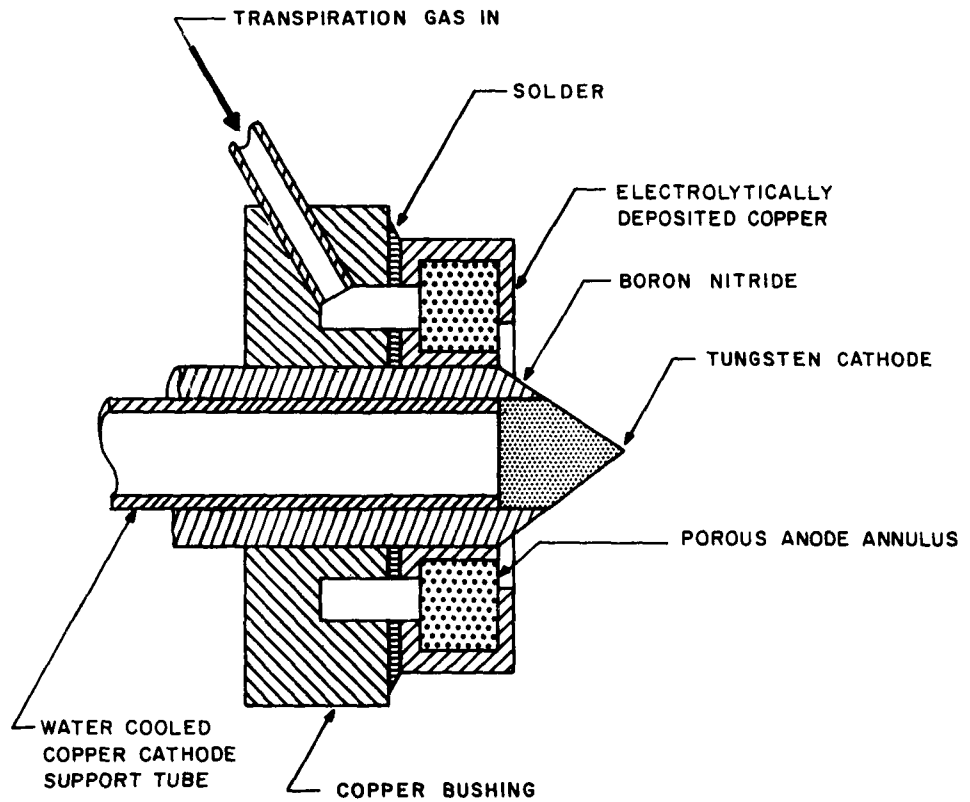


Fig. 46 Simplified Arc Assembly for Test of Sintered Spheroidized Tungsten Anode

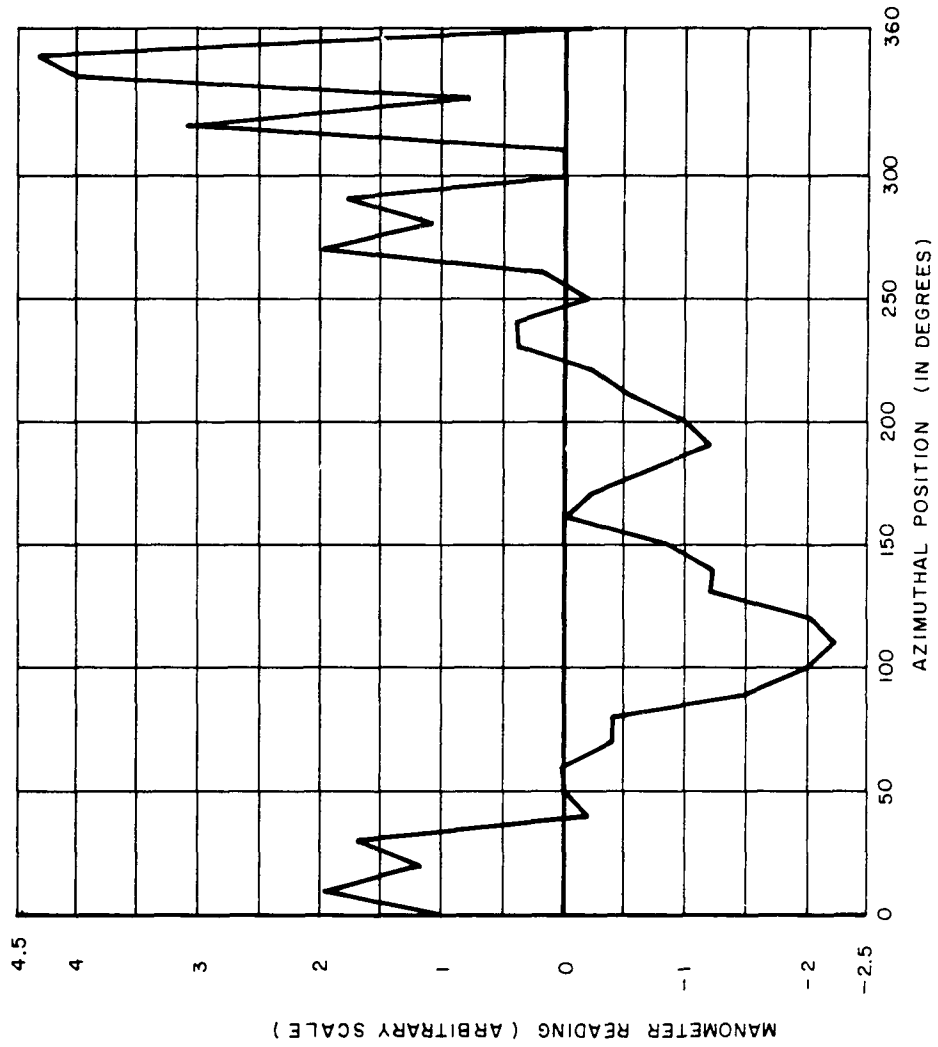


Fig. 47 Local Flow Probe Measurement:  
Interim Arc Assembly

#### IV. ANALYTICAL UNDERTAKINGS

Continuing search in the technical literature has served to focus our analytical efforts in the areas which are not already covered in the field and yet are most likely to be materially assisted by what has already been published. While the physics of high current electric arc without fluid motion has been rather thoroughly described (e.g., Finkelnburg and Maecker<sup>5</sup> and by Ecker<sup>6</sup>), the detailed mechanisms of arc behavior with fluid transpiration through the anode have been less completely discussed since the original work of Sheer, et al<sup>4</sup> which was followed up by Eckert et al<sup>7</sup>. Cann<sup>8</sup> laid out a ground work similar to that by Finkelnburg and Maecker to extend the understanding of the energy transfer processes by adopting the discipline of irreversible thermodynamics. But in neither case was application demonstrated to any significant extent. It is believed future advances will most likely come in this direction and we are pursuing it to a certain extent.

Within the porous medium the energy transfer processes are somewhat more tractable and consist principally of heat transfer from the material to the fluid, heat conduction from the anode sheath region to the material and, to lesser extents,  $I^2R$  heating within material and protective cooling. The physical parameters of interest here are the thermal conductivity of anode, flow permeability of anode, fluid flow rate, specific heat of fluid, electrical conductivity of anode, heat input from the sheath and the volume heat transfer coefficient between the anode and the fluid. The last parameter appears to not have been clearly defined. Grootenhuis<sup>9</sup> gives some experimental values of this parameter, which he denoted by  $h'$  was also made by a number of authors, e.g., Green<sup>10</sup>, Weinbaum and Wheeler<sup>11</sup>.

As a preliminary step, solutions were obtained for several cases of the steady-state coupled differential equations of heat conduction in the solid and convection in the fluid, in one-dimensional geometry:

$$h(T - t) = k(d^2T/dx^2) \quad (1)$$

$$h(T - t) = c_p \dot{M}(dt/dx) \quad (2)$$

where

- T - solid temperature
- t - fluid temperature
- h - volume heat transfer coefficient from solid to fluid
- $c_p$  - specific heat of fluid
- $\dot{M}$  - fluid mass flow rate

To arrive at the above equations, heat conduction in fluid was neglected which is usually three orders of magnitude below that in the solid. Also,  $h$ ,  $k$ , and  $c_p$  are assumed independent of temperature. The boundary conditions are:

at  $x = 0$  :  $dT/dx = 0$  (no heat input from upstream),  $t = t_0$

at  $x = a$  ;  $k(dT/dx) = Q =$  heat flux input from anode sheath.

Three solutions of interest are given in Figs. 48, 49 and 50. The parameter  $h$  differed among the three cases but all other parameters were given reasonable values as attainable under laboratory conditions. The significant result is that, as  $h$  increases, the fluid temperature lags increasingly behind the solid temperature. These cases are, in spite of their one-dimensional character, most pertinent to the present work with the fluid transpiration arc. For example, Sheer et al and Eckert et al reported anode face temperatures of the order of  $2000^\circ\text{C}$  which under their experimental conditions and in the light of our calculations must be associated with large differences in fluid and solid temperatures within the anode structure. It appears therefore that it is no longer safe to assume for all cases that large temperature drop between fluid and solid will not occur. This also suggests closer attention be paid to a precise determination of the  $h$  parameter.

A one-dimensional idealization may not always serve the purpose as there will always be a certain amount of heat exchange between anode and its holder but more importantly the heat input from the anode sheath is not necessarily uniform. As both Sheer and Eckert have shown the arc almost never terminates on the full surface of the anode. Thus for a more realistic description of the energy transfer model, axial symmetry is the next mode of approximating the various phenomena.

A three-dimensional mathematical description of energy exchange in the porous anode with fluid passage through arbitrary pressure gradients can be derived, as has been done by Bland<sup>12</sup>, to be the following:

$$\gamma \nabla^2 T = \frac{VP^2}{\lambda t} (T - t) = -\nabla P^2 \nabla \ln(t) = -\nabla^2 P^2 \quad (3)$$

#### Notation for (3)

$\lambda = (C_p \rho v)/h$  (a characteristic length)  
 $C_p =$  specific heat at const. pressure of gas  
 $\rho =$  density of gas  
 $v =$  flow velocity

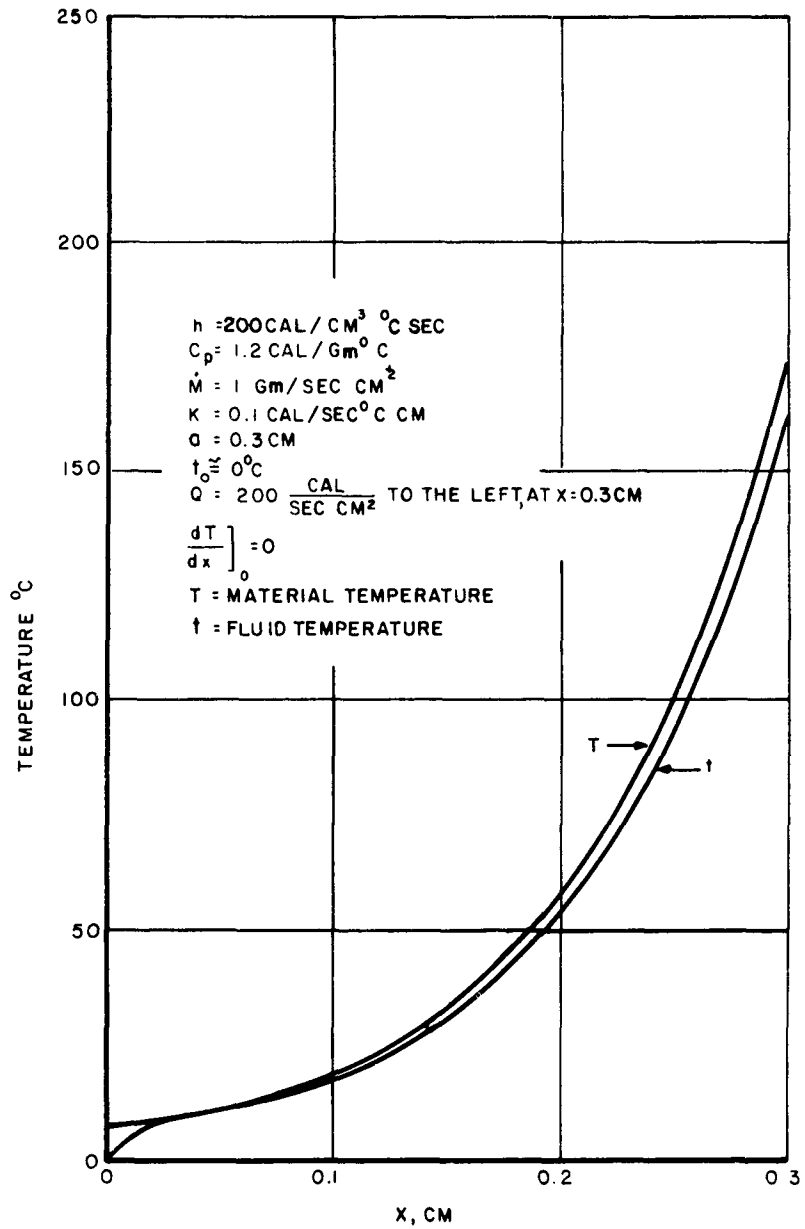


Fig. 48 One-Dimensional Fluid Transpiration Cooling, Case I

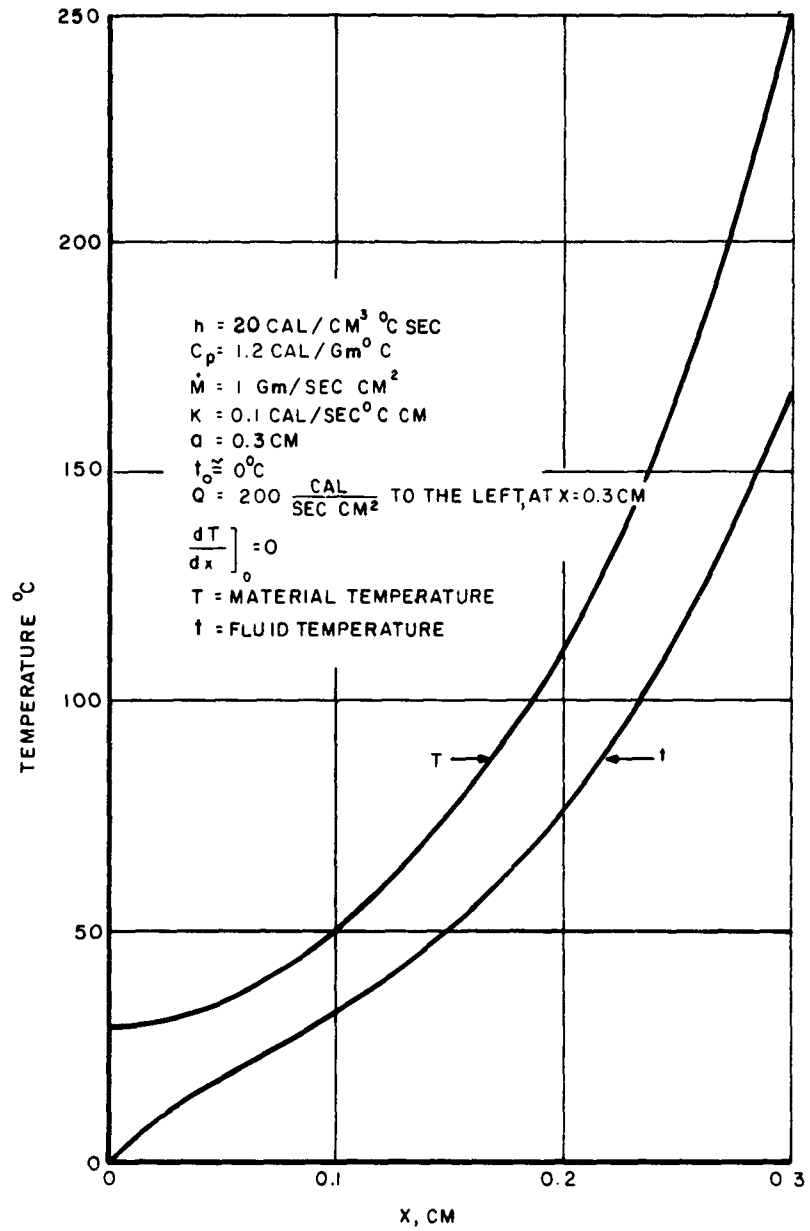


Fig. 49 One-Dimensional Fluid Transpiration Cooling, Case II

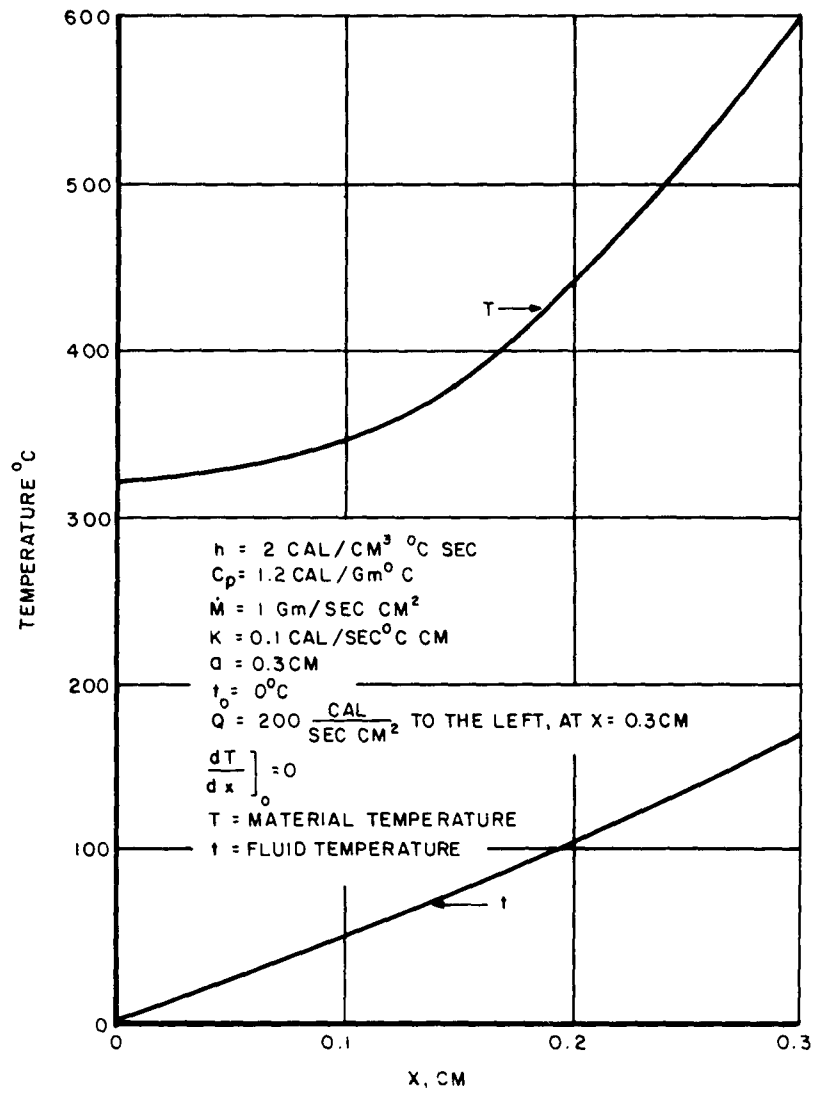


Fig. 50 One-Dimensional Fluid Transpiration Cooling, Case III

Notation for (3) (cont'd.)

$$\gamma = (2\mu\sigma)/(mC_p k)$$

m = Molecular Wt./Universal Gas Const.

$\mu$  = Coefficient of gas viscosity

$\sigma$  = effective solid conductivity

k = flow permeability in Darcy's Law

P = Pressure

No close solution has been found for the above set of equations and some sort of numerical scheme of solution may be resorted to. Bland had given hand-calculated results of cylindrical pieces adiabatic on the plane surfaces with the curved surfaces held at constant temperatures. Although those cases were different in boundary conditions from ours, it is instructive to note that his iteration procedures are susceptible to instability when a sufficiently wrong guess was made at the start of computation. This is obviously undesirable in the setup of modern computing machinery. A method has been worked out involving either the relaxation method or the squaring method of field computation in conjunction with a procedure of iteration and boundary conditions perturbation which should avoid instability and is therefore more suitable for automatic computers. The CUERL computer staff has assisted in working out such a computer program.

Among other things, with this computer program it will be possible to study the effects of temperature dependence of local flow rate on the extent of anode coverage by the arc. Similarly, it may be possible to find the conditions which a local hot spot will grow into failure proportion.

## V. SUMMARY AND CONCLUSION

The progress made during the first twelve months of the present studies on anode fluid transpiration arc has been reported in the preceding sections. The primary achievements of this period of work may be summarized as follows:

- (1) Design construction and shakedown for the electrode characterization program. These include measurements of porosity and pore-size distribution, thermal conductivity, gas flow permeability, local flow field variations, and microphotography
- (2) Evaluation of the following materials: sintered spheroidized tungsten, NC-50 and NC-60 graphites of National Carbon Co., PC-57 and PC-59 carbon of Stackpole Carbon Co. and stainless steel Feltmetal of Huyck Metals Corp.
- (3) Design and construction of the triple-cathode, cylindrical-anode transpiration arc test equipment and its instrumentation.
- (4) Preliminary analytical studies of transpiration cooling and the setting up of computer program for numerical solution of anode and sheath phenomena.

The execution of the continuing evaluation program has thus far indicated the sintered spheroidized tungsten to possess desirable properties as per the postulated criteria. This is not the whole purpose of the evaluation program, however, for the actual arc test will be the ultimate yardstick of success; to be correlated with the measured properties of the material used. This will be carried out soon since the arc assembly is now being put into operation.

Although only preliminary analytical results of the transpiration cooling studies are available at this point the indication is already clear that the temperature difference between electrode and fluid may at times be quite large. This may be taken to mean that the volume heat transfer coefficient is far more critical than is generally recognized.

## VI. REFERENCES

1. Gumenyk, V. S. and Lebedev, V. V., Phys. of Metals and Metallography, Vol. 11, October, 1961.
2. Engle, G. B. and Liggett, L. M., Research Labs., Speer Carbon Co.
3. National Carbon Co., The Industrial Graphite Engineering Handbook.
4. Sheer, C. et al, Tech. Note No. 1, Vitro Labs., June 16, 1961.
5. Finkelburg, W. and Maecker, H., Handbuch der Physik, Ed., H. Flugge, Vol. 22, Springer-Verlag, Berlin, 1956.
6. Ecker, G., "Electrode Components of the Arc Discharge," Ergebnisse der Exakten-Naturwissenschaften, Vol. XXXIII.
7. Eckert, Ernst R. G., et al, Thermische Untersuchung eines Elektrischen Hochstromlichtbogens mit Poröser, gasgekühlter Anode, Jr. Heat Mass Transfer, Vol. 5, Pergamon Press, 1962.
8. Cann, Gordon L., Energy Transfer Processes in a Partially Ionized Gas, Memo. No. 61, Guggenheim Aeronautical Lab., California Institute of Technology, June 15, 1961.
9. Grootenhuis, P., Jr. Royal Aero. Soc., Vol. 63, No. 578, February 1959.
10. Green, L., Jr. Appl. Mech., June 1952.
11. Weinbaum, S. and Wheeler, H. L., Jr. Appl. Phys., Vol. 20, January 1949.
12. Bland, D. R., Mathematical Theory of the Flow of a Gas in a Porous Solid and of the Associated Temperature Distributions, Proc. Royal Soc., Vol. 221. A, January 7, 1954.